BIOLOGICAL MODELS WITH A SQUARE WAVE DRIVING FORCE

TAUNIA LYDIA LYNN CLOSSON
B.Sc. in Chemistry, University of Lethbridge, 1999

A Thesis
Submitted to the School of Graduate Studies
of the University of Lethbridge
in Partial Fulfilment of the
Requirements for the Degree

MASTER OF SCIENCE IN CHEMISTRY

Department of Chemistry and Biochemistry
University of Lethbridge
LETHBRIDGE, ALBERTA, CANADA

To Michael,
for his constant support.

Abstract

Systems that require a driving force of some kind are very common in physical and biological settings. Driving forces in a biological context are usually referred to as rhythms, pulses or clocks. Here we are interested in the effect of adding a square wave periodic driving force to a biological model. This is intended to model inputs from biological circuits with all-or-none or switch-like responses. We study a model of cell division proposed by Novak and Tyson. Our switched input is intended to model the interaction of the mitotic oscillator with an ultradian clock. We thoroughly characterize the behaviour as a function of the durations of the active and inactive phases. We also study a model of vein formation in plant leaves proposed by Mitchison. Pulsed hormonal release greatly accelerates vein formation in this model.

Acknowledgments

I would like to thank my supervisor
Dr. Marc R. Roussel for his direction
and NSERC (National Science and Engineering
Research Council) for funding.

Table of Contents

List of Figures

List of Tables

Chapter 1

Introduction

Systems that require a driving force of some kind are very common in physical and biological settings.[1–8] For example, a swinging pendulum will oscillate back and forth until it stops due to friction. However, if a periodic force is used to drive the pendulum,[9] the pendulum may oscillate periodically without damping. The driven pendulum may also show more complicated dynamics such as chaos.[10] The focus here is on biological systems. Driving forces in a biological context are usually referred to as rhythms, pulses or clocks.[11–13] A very prevalent rhythm for most biological systems is a circadian rhythm[13–15] with a natural period of around 24 hours. These types of rhythms can usually be entrained to a light-dark driving force. There are numerous models of circadian rhythms that have been studied using a light-dark driving force.[16, 17] A slightly newer idea and less understood concept is an ultradian rhythm.[18–21] Ultradian rhythms are those with a period

of less then 24 hours. Both models that are investigated here incorporate an ultradian rhythm into models that did not take this type of behaviour into account. The first is a cell division cycle model. There is an apparent involvement of an ultradian rhythm in the cell division cycle.[19,22,23] The second model deals with auxin, a hormone in plants that contributes to vein formation in leaves. Plants have shown numerous circadian and ultradian rhythms experimentally.[13,24] Our interest is to see how the systems will behave when a periodic driving force is added. We chose a square-wave forcing to simulate periodic driving because there are many examples in biology of all-or-none responses, on-off switches or pulsatile hormone release.[25–30]

1.1 Terms and Techniques

The models that are studied here are nonlinear systems.[8] Nonlinear systems are difficult to solve analytically and have terms within them that are typically products, powers or functions of a variable x_i. Some examples of nonlinear terms are x_1x_2, $(x_1)^3$ or $\cos x_2$. Since nonlinear systems are not easily solved analytically, certain techniques have been developed to help interpret them. Some key concepts used to treat nonlinear models will be defined here. To help illustrate some of these definitions, the glycolytic oscillator proposed by Sel'kov (1968)[8] will be

used as a nonlinear example. The glycolytic oscillator is a two-dimensional model of the form:

$$\frac{dx}{dt} = -x + ay + x^2 y \tag{1.1}$$

$$\frac{dy}{dt} = b - ay - x^2 y \tag{1.2}$$

where x and y are the concentrations of ADP (adenosine diphosphate) and F6P (fructose-6-phosphate), and a,$b > 0$ are kinetic parameters.

A useful technique for understanding the qualitative behaviour of a system without doing a full analysis is a phase portrait. A phase portrait looks at the evolution of the different variables in a model with respect to one another. When there are only two variables, this plot is often referred to as the phase plane portrait since the plot is of the motion in a two-dimensional plane. Using the example of the glycolytic oscillator, the phase plane portrait is a plot of x versus y. For $a = 0.1$ and $b = 0.2$ the phase plane portrait has a stable fixed point at $x = 0.20$ and $y = 0.4286$ with all trajectories leading to it. The term fixed point, in reference to ordinary differential equations, represents equilibrium solutions or rest states. A locally stable fixed point represents a point in phase space that all nearby trajectories go towards. A locally unstable fixed point represents a point in phase space that all nearby trajectories will move away from. For $a = 0.08$ and $b = 0.6$ the phase plane portrait contains a limit cycle surrounding an unstable fixed point.

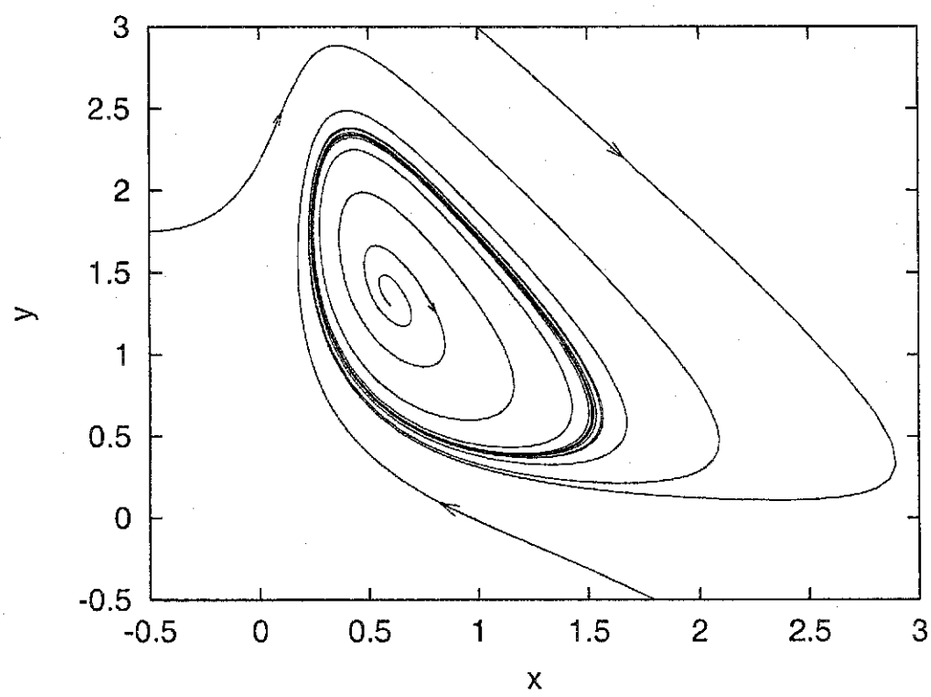

Figure 1.1: Phase plane portrait of a limit cycle for the glycolytic oscillator with $a = 0.08$ and $b = 0.6$.

This is illustrated in Figure 1.1. All trajectories whether started inside or outside the limit cycle will move toward and eventually follow the limit cycle.

Another technique to describe the behaviour of a system is a parameter space plot or a parameter plane plot. This plot is also sometimes referred to as a phase diagram, not to be confused with a phase portrait. These types of plots illustrate the different behaviour of a system due to the values of their parameters. In the

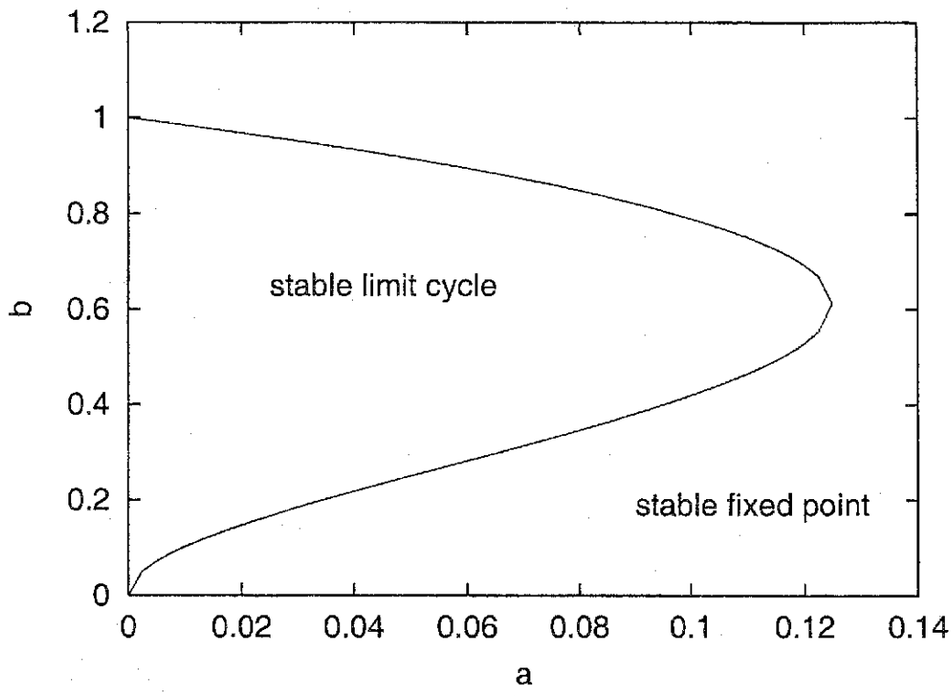

Figure 1.2: Parameter plane of the glycolytic oscillator with two regions corresponding to the different types of behaviour exhibited by this model.

glycolytic example, a parameter plane plot would be a plot of b versus a. The parameter plane for this example is illustrated in Figure 1.2. This parameter plane can distinguish the areas where the parameters give a stable fixed point or a stable limit cycle. The parameter values where these qualitative changes occur are called bifurcation curves.

The term chaos[4,8] is often used to mean different things. For this work, chaos

will be defined by two important ideas. 1) It arises in a deterministic system which exhibits aperiodic behaviour and 2) has exponential sensitivity to the initial conditions, making long term predictions of the system impossible. An example of a chaotic system using this definition is weather. The weather cannot be accurately predicted for more than a few days because the present conditions cannot be known to arbitrary accuracy. Because of the sensitive dependence on initial conditions which this system displays, forecasts diverge significantly from the real evolution of weather systems over a period of a few days.

Excitable systems[4,8] are quite important in the sciences. An excitable system can be described as having two properties: 1) It has a unique, globally attracting rest state. In other words, if the system is started from anywhere in phase space, the system will eventually go to a fixed point. 2) A large enough stimulus or perturbation will send the system on a long route through phase space before returning to its rest state. This second property is what distinguishes excitability from simple stability. Small perturbations below a certain threshold will return to its rest state by a rapid, direct path. Perturbations above this threshold will produce a long, indirect excursion through phase space before returning to the rest state. An example of a system that is excitable is a neuron.[4] When a neuron is injected with a small pulse of current, nothing dramatic happens. The neuron will increase

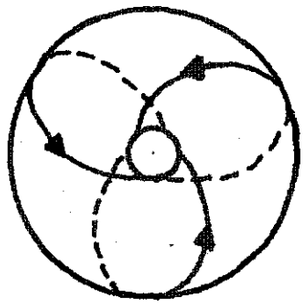

Figure 1.3: A two-dimensional representation of a $\frac{3}{1}$ trajectory on a torus.

its membrane potential slightly and then return to its resting potential. But when the neuron is injected with a large enough pulse of current, the neuron will "fire" producing a large voltage spike before returning to its resting potential.

Quasi-periodicity[4,8,31] is a term which is a bit harder to define. There are some systems whose trajectories lie on the surface of a torus in phase space. As the trajectory traverses the torus, if the trajectories meet and form a closed figure, the system is periodic. If for example, the trajectory winds around the torus three times while traversing the length of the torus once before meeting itself it is considered to have a rational winding number of $\frac{3}{1}$. A two-dimensional representation of a $\frac{3}{1}$ trajectory on a torus is given in Figure 1.3. A rational winding number represents periodic behaviour. However, if the winding number is irra-

tional, the system is considered quasiperiodic. This means that the trajectory on the torus never closes and the trajectory is dense on the torus.

Some molecular biology will also be discussed here. The convention for naming genes, mutations and gene products in this thesis will be as follows: Genes and mutations will be named using *italics* and gene products (proteins) will be named without italics usually with the first letter being capitalized. For example, Cdc7 is the protein product of the budding yeast *CDC7* gene.[32]

Chapter 2

Cell Division Cycle Model

2.1 Maturation Promoting Factor and Cell Cycle Control

A basic schematic of the different phases of the cell cycle is given in Figure 2.1. As our knowledge of the cell division cycle increases,[33–35] so too does the complexity of the models being proposed.[19,36–43] In particular one can look at the Maturation Promoting Factor (MPF) and its involvement in the cycle.[32,45,46] Our understanding of the structure and role of MPF in the cell cycle today began with the study of the cell cycle in yeast in the 1950's.[47] This research established some relationships between a number of different physiological parameters linked with growth and division. The next step came in the 1970's with the genetic studies of yeast and the isolation of cell division cycle (*cdc*) mutants.[48] This led to an explosion of genetic research on the cell cycle. As more and more *cdc* mutants were discovered and studied, the concept of a maturation promoting factor was

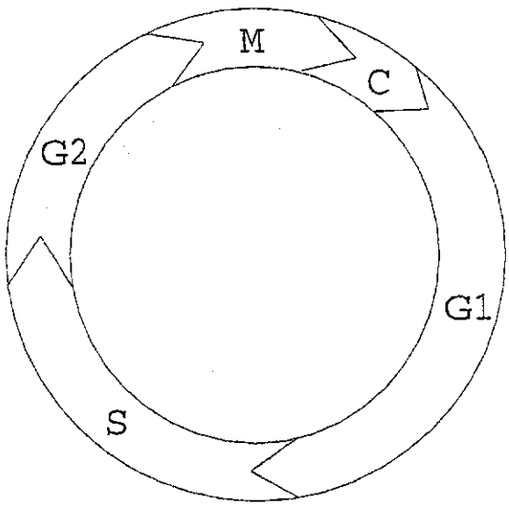

Figure 2.1: Schematic of the different phases in the cell cycle.[44] G1 is the primary growth phase of the cell, usually occupying a large portion of the cell's time. S is the phase in which the cell synthesizes a duplicate of the genome. G2 is the second growth phase in which preparation for mitosis occurs. These three phases make up what is usually referred to as the interphase. M is the phase that involves all the preparation for separation called mitosis. C is the phase where the cytoplasm divides, creating two daughter cells.

introduced. Initially, it was unclear what MPF was or if it was a group of steps or an individual molecule. This lead to further investigation to pinpoint what MPF was and how it worked.[49] It is now believed that MPF is a dimer of cyclin and Cdc2.[50,51] The activity of this dimer is dependent on its phosphorylation state. There are two phosphorylation sites which give four different states of MPF, only one of which is an active form. A schematic of MPF's role in the cell cycle is illustrated in Figure 2.2. From this schematic it is easy to see that some phosphorylation reactions inhibit the active form of MPF and some reactions activate it. The balance between this inhibition and activation makes for some interesting dynamics.

2.2 The Model

In the cell division cycle there are checkpoints which must be passed before mitosis can occur.[33,52] Checkpoints are points in the cell cycle at which a biochemical switch can halt mitosis. Checkpoints normally act through kinases and phosphatases which turn Maturation Promoting Factor (MPF) on or off. MPF is considered on when it has been phosphorylated in its activating residue and off when phosphorylated in any other way. When there is a sufficient concentration of active MPF mitosis is allowed, and when there is too low a concentration of active

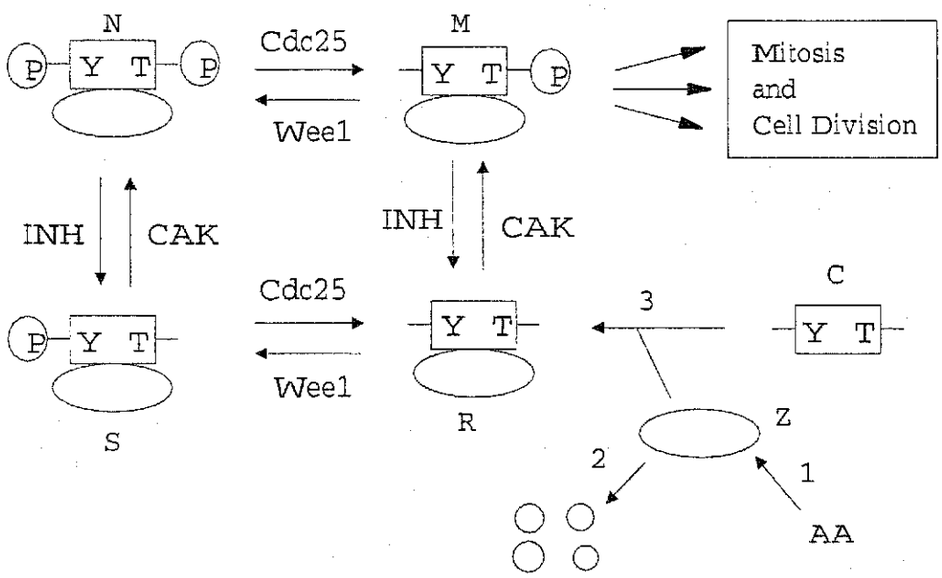

Figure 2.2: Schematic of MPF's role in the cell cycle (adapted from Novak and Tyson[45]). The oval (Z) represents cyclin, the rectangle (C) represents Cdc2 and the combination of the two represent the four different forms of MPF (M,N,S,R). The arms indicate the principal phosphorylation sites of Cdc2, tyrosine-15 (Y) on the left and threonine-167 (T) on the right. The different forms of MPF are distinguished by their phosphorylation states. MPF is active (M) when phosphorylated at the T site only. There are four different phosphatases and kinases involved in this process. INH is an inhibitory phosphatase, and Cdc25 is an activating phosphatase. Wee1 is an inhibitory kinase, and CAK is an activating kinase. Reaction 1 is the production of cyclin from amino acids (AA), reaction 2 is the degradation of cyclin and reaction 3 is the combination of cyclin and Cdc2. When active MPF (M) reaches sufficient concentration, mitosis and cell division are initiated.

MPF mitosis is halted.

There is a simple mathematical model describing the chemistry for mitotic control proposed by Tyson and Novak[45] derived from early embryonic development in amphibians. This model consists of two differential equations:

$$\frac{du}{dt} = k_1 g - u(k_2 + k_3 u^2 + k_{\text{wee}}) + (k_4 + k_5 u^2)(gv - u) \tag{2.1}$$

$$\frac{dv}{dt} = k_1 - v(k_2 + k_3 u^2) \tag{2.2}$$

where u is the concentration of active MPF, and v is the concentration of cyclin, both scaled by the total amount of Cdc2. The k_i's are rate constants, g is a constant related to a ratio of activity of INH and CAK and k_{wee} describes the activity of the inhibitory Wee1 kinase. These differential equations are a reduction of a more complicated group of 11 ordinary differential equations. A major simplification in this model was to assume that the total Cdc2 levels remain constant in the cell.

For some values of the parameters, the system has a stable limit cycle, and for some other values the system goes to an equilibrium. When the system has a stable limit cycle it is modeling a cell involved in repeated, regular mitoses representative of early embryonic development. When the system goes to equilibrium it is modeling a cell that is G2 arrested, or not involved in mitosis. Both of these types of behaviours are interesting, but do not explain all aspects of cell mitotic behaviour, including checkpoints. For example, a cell may be G2 arrested for

a period of time, and will eventually be given the signals needed to pass certain checkpoints to initiate mitosis. An example of this is a cell that is required to grow to a sufficient size before it can divide again.[53,54]

It has been found that many biological checkpoints exhibit switch-like behaviour.[26,55,56] To incorporate a checkpoint into this model, a parameter that could likely exhibit this switch-like behaviour was needed. Since kinases and phosphatases are known to act like switches, the parameters k_{wee} and g were looked at. The parameters k_{wee} and g are both given constant values in the Tyson-Novak model. The Wee1 kinase is singled out by Novak and Tyson as an important inhibitory kinase involved in mitotic checkpoints, while the INH and CAK proteins could not as of yet be linked directly to mitotic checkpoints. Price *et al.* and Russell *et al.* also singled out *wee1* as important for division.[57,58] Therefore, k_{wee} is chosen as the switch. When $k_{\text{wee}} = 1.5$ the system has a stable limit cycle with a period of about 34.35 minutes. When $k_{\text{wee}} = 3.5$ the system is excitable with both u and v going to equilibrium. To simulate the switch-like character of the MPF checkpoint, we switch between these two states of k_{wee}. Switching between a state of periodic oscillations and a state of G2 arrest is chosen to try and simulate cells being able to exit their G2 arrested state, and return to an oscillatory state for a time to undergo mitosis. The switch that we add is independent of the cell cycle

events which resembles the idea of an ultradian clock.[18]

Ultradian rhythms seem to act in numerous biological events. It is unclear what the mechanism is for these ultradian clocks. However, there is a lot of experimental evidence that the cell cycle is governed by more than one clock each having a distinct rhythm and the implications of such rhythms have been discussed.[15,18–20,59,60] The two most common behaviours associated with the interactions between ultradian and cell cycle clocks are entrainment and chaos.[16]

2.3 Computer Simulations and Data Collection

2.3.1 Periodic Driving

An on-off switch for k_{wee} is implemented as follows. The switch is on when $k_{wee} = 1.5$ and off when $k_{wee} = 3.5$. To obtain a periodic driving signal, we use:

$$m(t) = t - \lfloor \frac{t}{T} \rfloor T \tag{2.3}$$

where the driving period $T = \tau_{on} + \tau_{off}$, $\lfloor\ \rfloor$ is the floor function* and τ_{on} and τ_{off} are the durations for which the switch is on or off. The function $k_{wee}(t)$ is then defined to be 1.5 when $m(t) < \tau_{on}$ and 3.5 when $m(t) \geq \tau_{on}$. This produces a square wave to simulate an on-off switch with variable periods.

*The floor function of x gives the largest integer less than or equal to x.

2.3.2 Time Series Data

We are interested in the evolution of u in time. There are three types of possible behaviours. There can be entrainment, in which there is a repeating pattern in relation to the driving period. There can also be chaos,[61] in which no pattern can be found and a positive Lyapunov exponent is calculated.[62,63†] Lyapunov exponents[8,64] are a measure of a system's sensitivity to initial conditions. If a positive Lyapunov exponent is calculated then, provided a few other technical conditions are met, the system is chaotic. Or there can be quasi-periodicity,[31,65] in which no pattern can be found but the system is not chaotic, having only negative Lyapunov exponents. A way of categorizing these different behaviours is by calculating different winding numbers.[66,67] A system which is entrained will have rational winding numbers, and a system that is chaotic or quasi-periodic will have irrational winding numbers. However, in this study winding numbers are only calculated for the entrained cases to differentiate between the different patterns found. Labeling peaks of the repeating unit is also used as a technique to differentiate between the patterns. This labeling of peaks is often referred to as symbolic dynamics.[68] Figure 2.3 illustrates how peaks are labeled and how the peak pattern is defined. When $u > 0.1$ mitosis is initiated and when $u \leq 0.1$ mi-

†Lyapunov exponents were previously calculated by Marc Roussel and are reported elsewhere.

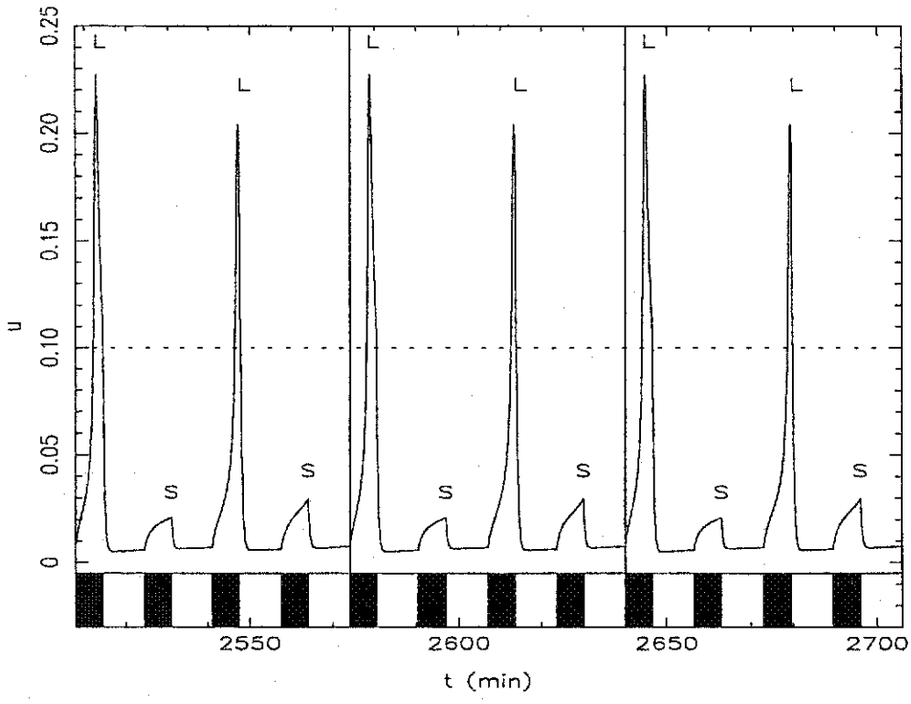

Figure 2.3: Time series plot of species u for $\tau_{on} = 6.5$ and $\tau_{off} = 10$. The repeating pattern is separated by vertical lines and the different peaks are labeled depending on their value. Peaks above $u = 0.1$ are labeled with an L (large) and peaks below $u = 0.1$ are labeled S (small). The periodic driving for this system is illustrated by the black and white boxes along the bottom axis. The black boxes represent the time the switch is on ($k_{wee} = 1.5$) and the white boxes represent the time the switch is off ($k_{wee} = 3.5$). The peak pattern for this system is defined as the peak labels of all the peaks within a repeating unit. For consistency, each set of labels is always started with a small peak S (unless only large peaks exist) and then the set is abbreviated if there is a repeating pattern within the pattern. For example, this system has the peaks LSLS in one repeating unit. To begin the pattern with a small peak it is rearranged to be SLSL. Since there is a repeating unit of SL in this pattern that occurs twice we then rearrange the pattern to get $(SL)^2$.

tosis is not initiated.[‡] Therefore, responses that are above 0.1 are labeled L for large peaks and responses that are below 0.1 are labeled S for small peaks. Both are relevant to the dynamics of the system, but the peaks that initiate mitosis are of greater interest. The two winding numbers calculated are defined as:

$$\omega_{\text{all}} = \frac{\text{\# of maxima in } u}{\text{\# of driving periods}} \tag{2.4}$$

$$\omega_a = \frac{\text{\# of maxima in } u \text{ above } 0.1}{\text{\# of driving periods}} \tag{2.5}$$

for each repeating unit. These fractions are not simplified so that the differences between each pattern can be distinguished. For example, in Figure 2.3 the winding numbers are $\omega_{\text{all}} = \frac{4}{4}$ and $\omega_a = \frac{2}{4}$. These are not simplified to $\omega_{\text{all}} = \frac{1}{1}$ and $\omega_a = \frac{1}{2}$ because the four peaks that occur in the four driving periods are all different and should be distinguished from a pattern where there is only one large peak in two driving periods for a repeating unit.

To calculate the type of data in which we are interested, a computer simulation program was developed. An implicit Runge-Kutta method[§] is used to integrate the two differential equations of our modified Tyson-Novak model. The initial

[‡]The value of $u = 0.1$ was chosen somewhat arbitrarily as there is no clear experimental evidence as to the MPF threshold required for mitosis. Similar arbitrary choices are commonly made in cell cycle models.[69] However, choosing a different value within a small range of this number would have resulted in qualitatively similar results since peaks leading to mitosis are generally much larger than those that do not.

[§]A description and the implementation of the implicit Runge-Kutta method are given in Appendix A.

Table 2.1: Parameter values for our modified Tyson-Novak model with a time scale in minutes.

Parameter	k_1	k_2	k_3	k_4	k_5	g
Value	0.01	0.01	10	0.04	100	0.9

stepsize[¶] (h) for the implicit Runge-Kutta method is a user-defined parameter. Different values of τ_{on} and τ_{off} are also user-defined parameters. The system is started with the initial values of $u(0) = 0$, $v(0) = 0$ and $k_{wee}(0) = 1.5$. All other values for the rate constants are identical to Novak and Tyson values which are contained in Table 2.1. Before a pattern can be found, the system must first reach stationarity.[4,70‖] To ensure that sufficient time has passed for the time series to become stationary, values of u are v are calculated for a time of $100T$ or 2000 time units, whichever is larger. These points are not stored since we are interested in the system after it has reached stationarity. Values are then calculated and stored for an additional time of $50T$, or at least 1000 time units. Since we are only

[¶]In the simulation program the system is integrated at least twice. The first time the system is integrated using the initial stepsize defined by the user. Any subsequent runs are integrated using a smaller stepsize for comparison.

[‖]Stationary state refers to a state of equilibrium or rest. When a system has reached a stable fixed point or a stable limit cycle, it is considered stationary. For systems that do not have a stable fixed point or a stable limit cycle (eg. chaotic) it is considered stationary when two long sets of data from different areas in the data have identical statistical properties, ie. average, winding number, etc. If they do not have identical statistical properties, the system has not reached stationarity and a longer transient is needed.

interested in the responses of u, we then collect the points where $u(t)$ are maxima for the required range of t. From these maximal values we then do a comparison to find if there is a repeating pattern.

To find a repeating pattern with respect to T we compare responses in adjacent sections of integer multiples of the driving period. If we look at the system with $\tau_{on} = 9$ and $\tau_{off} = 5$ from Figure 2.4 this can be better illustrated. Since $100T < 2000$ the values are taken starting at time 2000. An integer n is defined to keep track of the number of driving periods we are comparing for a repeating unit. Once the maxima are collected the points found between 2000 and $2000 + nT$ are compared with the points found between $2000 + nT$ and $2000 + 2nT$, to see if they are sufficiently similar. If there are a different number of maxima found in the sections, then they are not similar. If there are the same number of maxima found in the sections then each set of maxima for the two sections are compared individually. For example the first maximum found between 2000 and $2000 + nT$ is compared with the first maximum found between $2000 + nT$ and $2000 + 2nT$, or the first and second regions respectively. This is illustrated in Figure 2.4c. All consecutive points are compared in like manner. The criterion used to compare the points in the two regions is:

$$c = (t_2 - t_1 - nT)^2 + \left(\frac{u_2 - u_1}{u_2 + u_1}\right)^2 \tag{2.6}$$

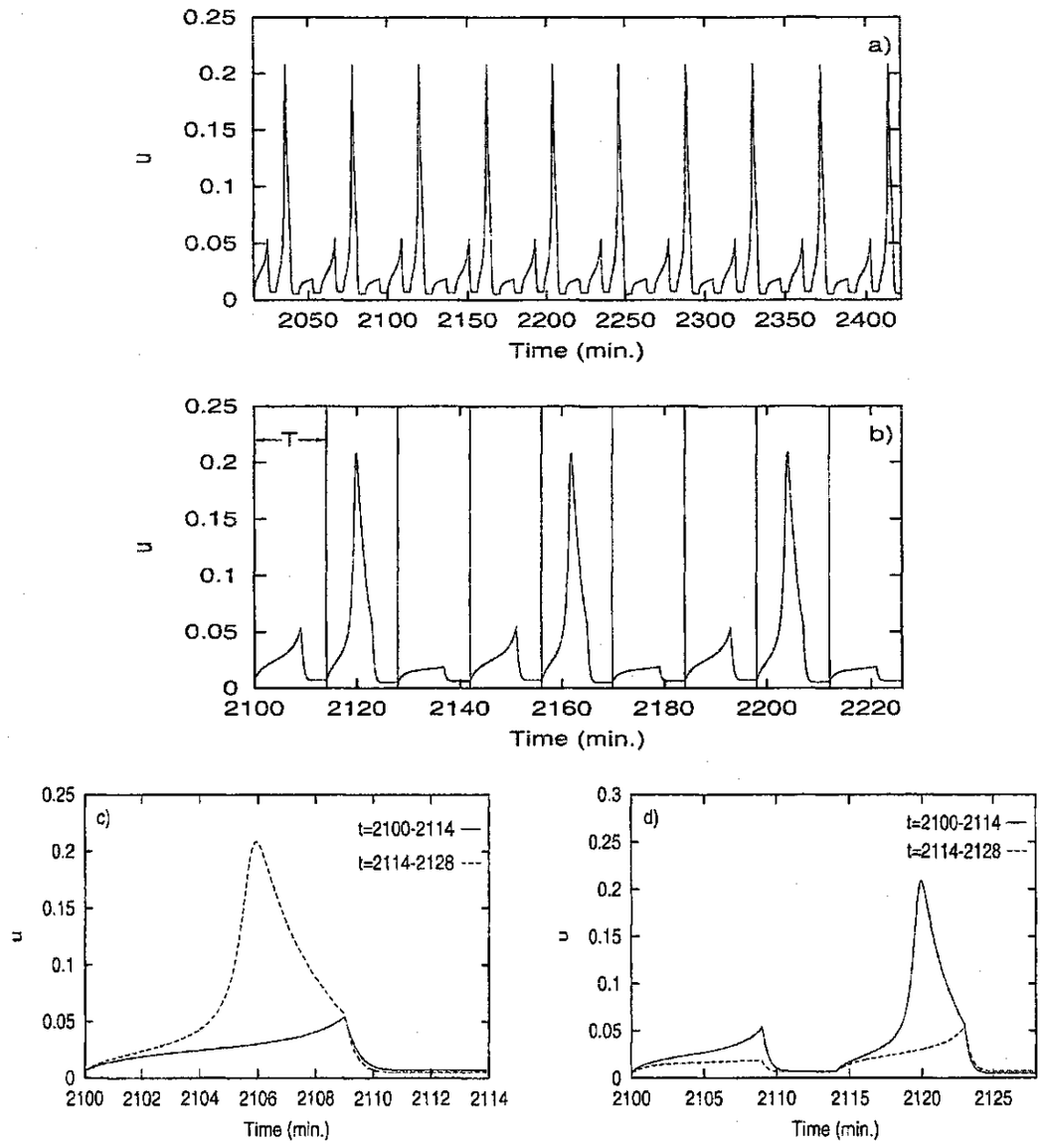

Figure 2.4: Simulation using $\tau_{on} = 9$ and $\tau_{off} = 5$. a) The evolution of u with time. b) Driving period T related to $u(t)$. c) Comparing the responses when $n = 1$ to check for a pattern. d) Comparing the responses when $n = 2$ to check for a pattern. In this case, an S^2L pattern is found when $n = 3$.

where the subscripts denote the region. For example, if the first maximum (t,u) in one driving period is compared with the first maximum in the next driving period, the maximum in the first region is given the subscript 1 and the maximum in the second region is given the subscript 2. If $c \leq 2h^2$, then the maxima are considered the same. If $c > 2h^2$, then the maxima are considered to be different.** When all the maxima are similar then the number of responses are calculated for the time nT in which the unit repeats. If they do not match when $n = 1$, which is the case for our example as shown in Figure 2.3c, then the next group of adjacent time periods ($n = n + 1$) are compared, as shown in Figure 2.3d. This is repeated until a pattern is found or until $n = 25$ when all the data for u collected have been looked at. In this example a pattern is found when $n = 3$.

The whole process is then repeated using a smaller stepsize of $h = \frac{h}{2}$. The answers from both cases are compared and if they are the same the key data are output. If they are not the same, the whole process is again repeated with a reduction in stepsize of $h = \frac{h}{2}$.

Simulations are performed for a range of τ_{on} values from 0.5 to 35 going up

**The integrator increments time by the stepsize h. Therefore, the error incorporated with the first term of c is at most h, which is then squared. If two maxima are similar, then the second term should be of order h^4, which is the magnitude of the numerical error of the implicit Runge-Kutta method.[71] This term is then squared giving an error much smaller then the first term. So the intrinsic error of c is of the order of h^2. If two peaks are nonincidental, we find empirically that $c > 2h^2$.

by 0.5 and for τ_{off} from 0.25 to 20 going up by 0.25. Most of the data are collected in the manner described above. All data acquired for a (τ_{on}, τ_{off}) pair in which the program found no pattern are compared with the Lyapunov exponents for the same system. If the Lyapunov exponents are positive[††] then it is confirmed that no pattern exists. However, in a handful of cases the Lyapunov exponents are negative and some extra exploring of those cases is required. This exploring led to some minor variations of the original program. One variation used a longer transient and stored more data. This meant having larger n's. The other variation involved starting at a significantly smaller stepsize, h. In the very small number of cases where a pattern is still not found using the above variations and the Lyapunov exponents are negative, it is concluded that these systems are probably quasi-periodic. Overall the simulations and data collection worked well.

2.3.3 Next Return Maps and Power Maps

Another useful technique for interpretation of the simulation data is the use of next return maps and power maps. The way in which these maps are defined and how they are implemented will be discussed in this section. Here, next return maps are defined by plotting subsequent angles. The angles are defined somewhat

[††]Recall that positive Lyapunov exponents denote a chaotic system.

arbitrarily from points on the trajectory in a (u,v) phase space plot and a line segment picked as a reference. This is sensible when the attractor is like a limit cycle in that there exists a point in phase space which is surrounded by the attractor and around which the trajectories always move in the same direction.[7] In this case, these criteria are met. The points on the trajectory are chosen as the values of u and v immediately after the switch is turned from on to off, i.e. when k_{wee} is switched from 1.5 to 3.5. The reference line is chosen for each individual case by choosing a reference point in the (u,v) plane which lies inside a loop made by the trajectory points described above and drawing a horizontal line from this reference point to the right. The angle θ, corresponding to a point in the (u,v) plane is defined relative to this line. This can best be described by example in Figure 2.5a. Simulations are run similarly to the time series simulations using the implicit Runge-Kutta method to integrate the two differential equations. There is an initial transient period where data are not collected. After this transient period, data are only collected for the points u and v directly after the switch is turned off. A reference point is defined by the user and the angles are then calculated from the (u,v) points collected. The data are arranged in two columns of θ_i and θ_{i+1} which are then plotted as a next return map. An example of a simple next return map is given in Figure 2.5b. These next return maps are mostly used to study the

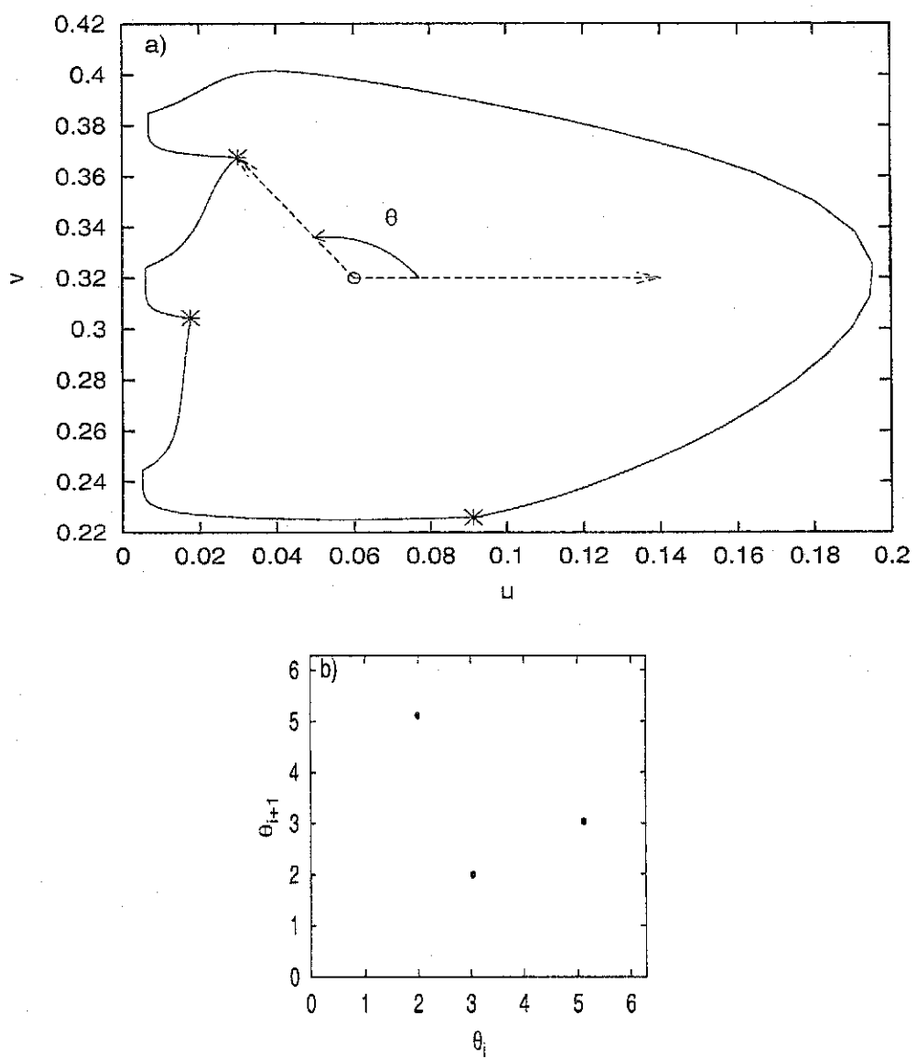

Figure 2.5: Next return map examples using the system with $\tau_{on} = 9$, $\tau_{off} = 3$, $\omega_{all} = \frac{3}{3}$ and a S^2L peak pattern: a) Phase plane plot illustrating how the angles are defined in the next return maps. The three stars are points on the trajectory immediately after the switch has been turned off. The open circle is the reference point. The angle, θ, is defined between the reference line drawn from the reference point and the trajectory point. b) An example of a next return map illustrating the three different angles corresponding to the three points on the trajectory.

chaotic regions.

A variation on the next return maps are power maps. Power maps display the data at a certain power of the previous data. For example a power-3 map plots θ_i against θ_{i+3}. The data for power maps are collected in the same fashion as for the next return maps, the only difference being that when the angles are collected for a power-3 map plot, only every third angle is used. The value of the power applied to the map is a user defined quantity. A power-3 map of the data from Figure 2.5 would consist of a single point on the line $\theta_i = \theta_{i+3}$. Power maps are used to investigate the routes to chaos.

2.4 Results

2.4.1 Winding Numbers and Peak Patterns

This section deals only with the entrained or phase locked systems that have periodic behaviour and can be classified with a rational winding number. Phase locking is quite common in many biological systems.[72] For example, experiments have been done where the respiratory system of mammals can be entrained to a mechanical ventilator.[73,74] Also, when there is a large cell population, there sometimes needs to be some form of synchronization[69,75–77] to coordinate different events. For example, in early development the growth of limbs needs to be

coordinated so that they each grow at approximately the same rate. It has been theorized that a clock can be used to fit this purpose.[12,18,60]

The winding numbers (ω_{all}) calculated from all the responses fall into three categories. There are winding numbers equal to one, equal to a value less than one and equal to a value greater than one. Examples of the three ω_{all} categories are given in Figure 2.6a-c. To understand the fundamental differences between these categories, it is useful to look at the phase space trajectories of the two behaviours the model switches between. Figure 2.7 shows the limit cycle and the $\dot{u} = 0$ nullcline when $k_{wee} = 1.5$ and the fixed point when $k_{wee} = 3.5$. When the switch is on the system follows the limit cycle. When the switch is switched off the system moves towards the fixed point until it is switched back on, at which point the system has to move back towards the limit cycle. The distance between the limit cycle and fixed point is large enough that it takes some time to move all the way from one to the other. As time progresses u will oscillate from high to low values when moving along the limit cycle and will go to a low value when moving towards the fixed point. Therefore, when the switch is left on, the system will oscillate with a period of about 34.35 minutes. However, when the system is turned off, the value of u will quickly go down. This can be seen in Figure 2.3 when the bottom boxes representing the switch goes from black to white (on to

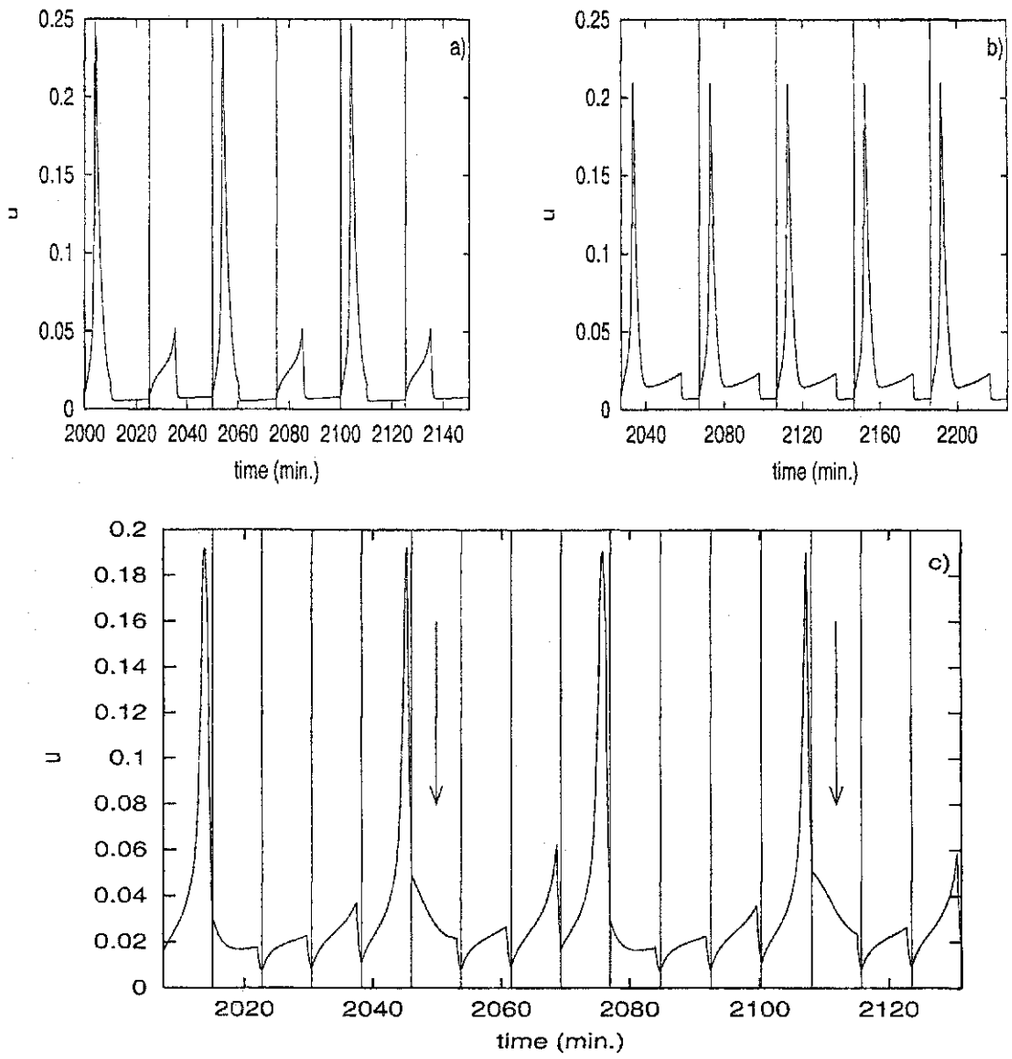

Figure 2.6: Time series plots showing the different categories of ω_{all} with the driving periods divided by vertical lines (where the switch turns from off to on). a) $\omega_{all} = 1$ for $\tau_{on} = 10$ and $\tau_{off} = 15$. There is one peak per driving period. b) $\omega_{all} > 1$ for $\tau_{on} = 30.5$ and $\tau_{off} = 9.25$. There is more than one peak per driving period. c) $\omega_{all} < 1$ for $\tau_{on} = 7$ and $\tau_{off} = 0.75$. There are some driving periods that do not have any peaks which are illustrated by arrows. These have the value of u declining and then before it can rise, the value of u drops off sharply.

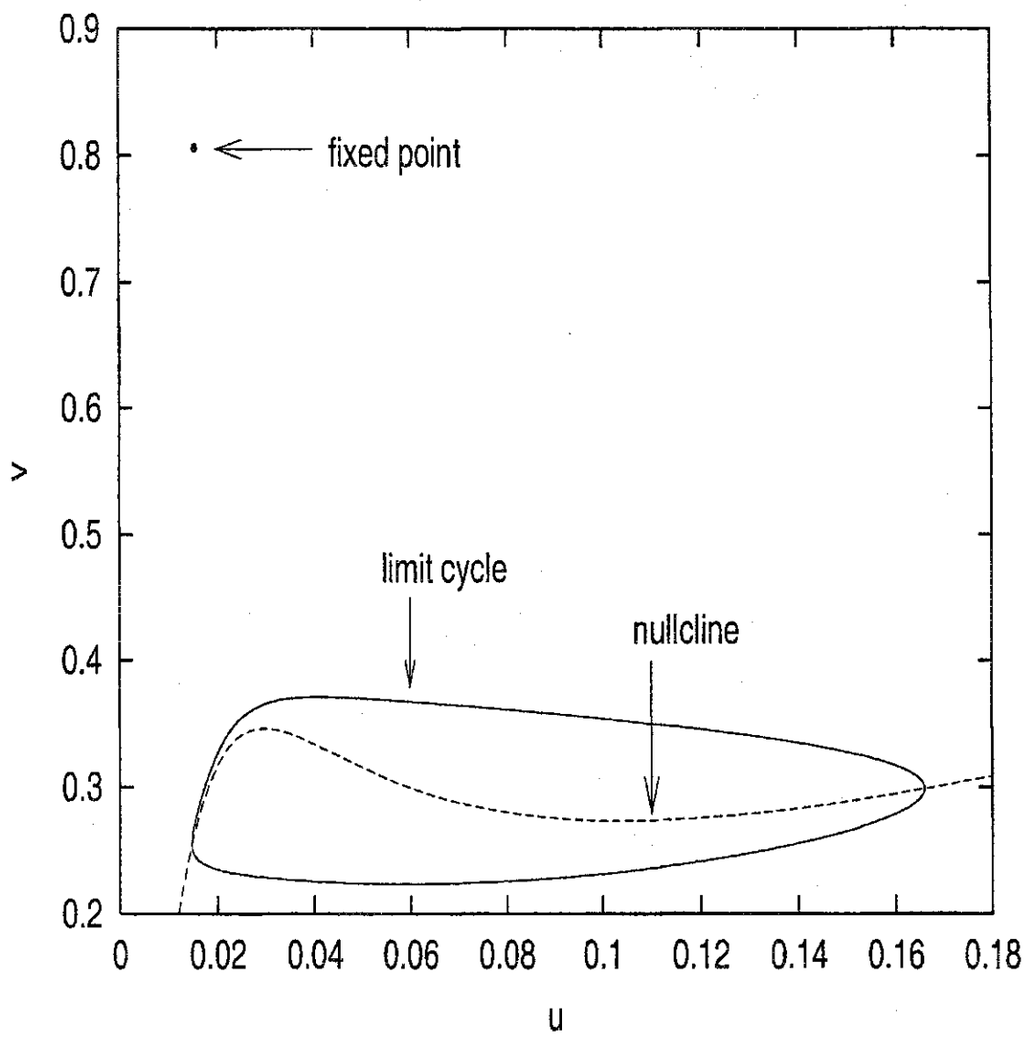

Figure 2.7: The phase space diagram of the Tyson-Novak model without switching. The system follows a limit cycle when $k_{wee} = 1.5$ and goes to a fixed point when $k_{wee} = 3.5$. The dotted line represents the u-nullcline which divides the limit cycle into two sections. Above the nullcline the value of u is increasing and below the nullcline the value of u is decreasing.

off) the value of u quickly drops. When $\omega_{all} = 1$ the switching of the parameters is fast enough that only one response can occur during one driving period. To put it another way, the system is not left on the limit cycle long enough to peak more than once. When $\omega_{all} < 1$, which rarely occurs, the switch is being turned on and off too rapidly for a response to occur each driving period. This only occurs at small values of τ_{on} and τ_{off} because at such small values of both, the system occasionally cannot spend enough time moving along the limit cycle for a response to occur before the switch is turned off again. For example, if the switch is on and the system is moving along the limit cycle below the nullcline (u is decreasing) and the switch is then turned off, making u decrease, a maximum will not occur during this driving period. And when $\omega_{all} > 1$ the driving period is long enough to allow more responses to occur. These three categories can be visualized in different regions on the parameter plane in Figure 2.8 in relationship to the regions with irrational winding numbers. There are two distinctly different regions of $\omega_{all} > 1$ on this plot. There is a subtle difference between the two regions. The region that covers the top right corner has a value of $\omega_{all} = \frac{2}{1}$ which corresponds to two peaks per driving period, while the other region has values of ω_{all} between 1 and 2 which correspond to some of the driving periods with two peaks and some of the driving periods with one peak.

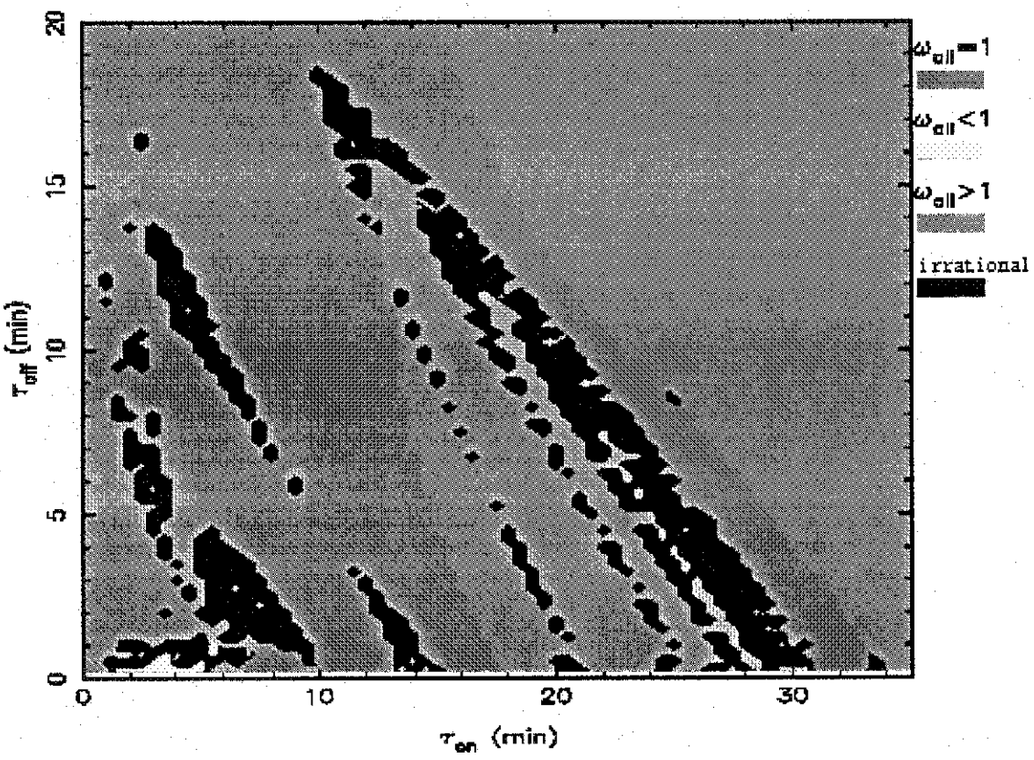

Figure 2.8: Regions of the τ_{on} and τ_{off} parameter plane which denote the different behaviours of ω_{all} compared to the region where the winding number has an irrational value.

The other winding numbers (ω_a) calculated from the responses that lead to mitosis are generally small rational ratios less than or equal to one. This is illustrated in Figure 2.9a along with the corresponding peak patterns. It is important to note here the behaviour of the system at a constant value of T. When looking at the winding numbers of these diagonal slices of constant T, it is clear that the system is sensitive to the actual values of τ_{on} and τ_{off} and not just to the total period. Table 2.2 shows the winding numbers for three different examples of constant T. The diagonal section for $T = 20$ shows similar behaviour with most having an $\omega_a = \frac{1}{2}$. The other two examples show a lot more variation in behaviour along their diagonal. The general trend of the different sections displayed in Figure 2.9 do follow a diagonal looking trend, however the variations of specific diagonals are enough to see that the different values of τ_{on} and τ_{off} are more important than the sum of the two.

Regions left blank in Figure 2.9a display more complex phase locking, chaotic or quasi-periodic behaviour. In general, the chaotic regions fall in the middle of the blank regions, and the more complex phase locking are part of a route taken towards these chaotic regions. Quasi-periodic behaviour, which is rare in our model, is mostly found near the edges of the chaotic regions.

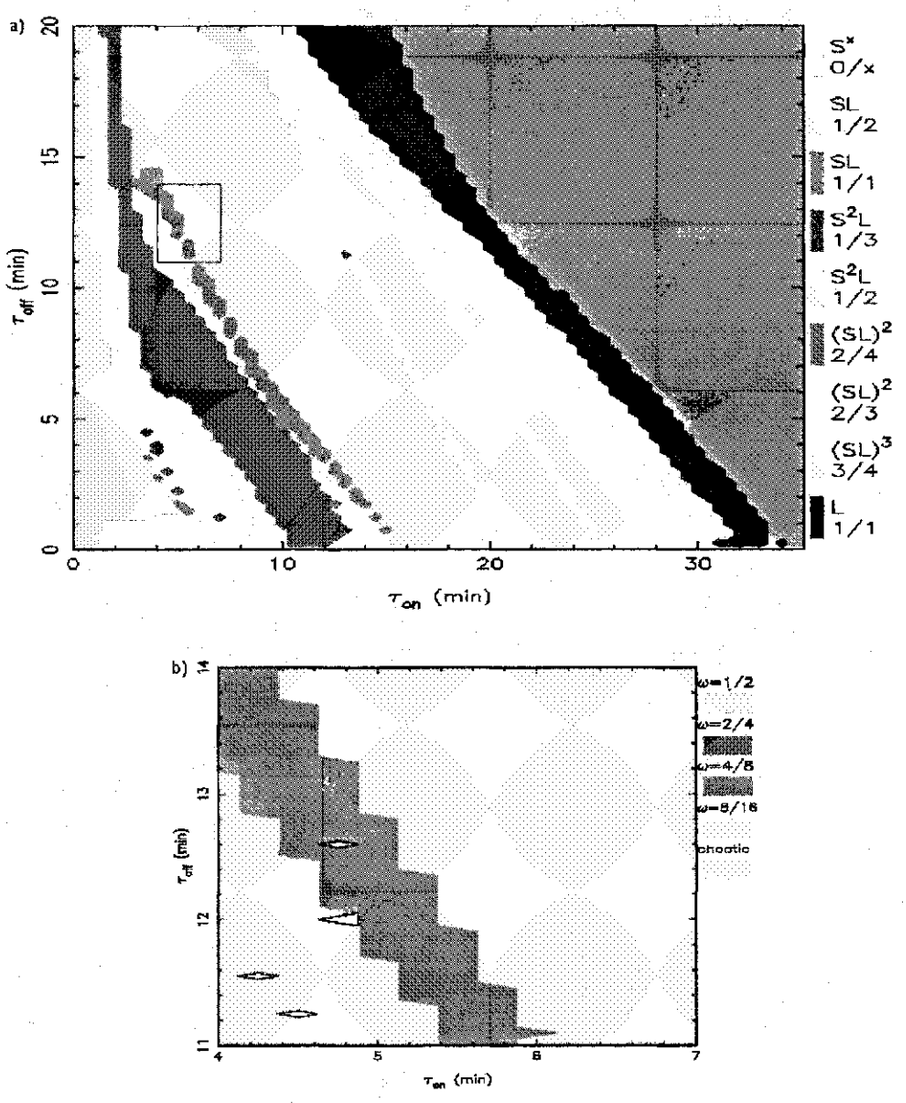

Figure 2.9: Parameter plane plot: a) Regions in τ_{on} and τ_{off} parameter plane which denote the different ω_a's and peak patterns. Regions left blank display more complex phase locking, quasi-periodic or chaotic behaviour. b) Blown up region of the τ_{on} and τ_{off} parameter plane illustrating a period doubling route to chaos. Regions left blank exhibit different phase locking patterns.

Table 2.2: Diagonal comparison of T using winding numbers for three different values of of T.

$T = 15$			$T = 20$			$T = 25$		
τ_{on}	τ_{off}	ω_a	τ_{on}	τ_{off}	ω_a	τ_{on}	τ_{off}	ω_a
0.5	14.5	0/1	0.5	19.5	0/1	5	20	1/2
1	14	1/7	1	19	1/5	5.5	19.5	1/2
1.5	13.5	1/5	1.5	18.5	1/4	6	19	1/2
2	13	1/4	2	18	1/3	6.5	18.5	1/2
2.5	12.5	1/3	2.5	17.5	1/2	7	18	1/2
3	12	1/3	3	17	1/2	7.5	17.5	1/2
3.5	11.5	1/3	3.5	16.5	1/2	8	17	1/2
4	11	irrational	4	16	1/2	8.5	16.5	1/2
4.5	10.5	irrational	4.5	15.5	1/2	9	16	1/2
5	10	irrational	5	15	1/2	9.5	15.5	1/2
5.5	9.5	irrational	5.5	14.5	1/2	10	15	1/2
6	9	irrational	6	14	1/2	10.5	14.5	1/2
6.5	8.5	irrational	6.5	13.5	1/2	11	14	1/2
7	8	irrational	7	13	1/2	11.5	13.5	1/2
7.5	7.5	irrational	7.5	12.5	1/2	12	13	3/4
8	7	irrational	8	12	1/2	12.5	12.5	3/4
8.5	6.5	4/7	8.5	11.5	1/2	13	12	3/4
9	6	irrational	9	11	1/2	13.5	11.5	irrational
9.5	5.5	1/2	9.5	10.5	1/2	14	11	2/3
10	5	1/2	10	10	1/2	14.5	10.5	2/3
10.5	4.5	1/2	10.5	9.5	1/2	15	10	2/3
11	4	1/2	11	9	1/2	15.5	9.5	2/3
11.5	3.5	1/2	11.5	8.5	1/2	16	9	2/3
12	3	irrational	12	8	1/2	16.5	8.5	2/3
12.5	2.5	irrational	12.5	7.5	1/2	17	8	2/3
13	2	irrational	13	7	1/2	17.5	7.5	2/3
13.5	1.5	irrational	13.5	6.5	1/2	18	7	2/3
14	1	irrational	14	6	1/2	18.5	6.5	2/3
14.5	0.5	irrational	14.5	5.5	1/2	19	6	2/3
			15	5	1/2	19.5	5.5	2/3
			15.5	4.5	1/2	20	5	2/3
			16	4	1/2	20.5	4.5	2/3
			16.5	3.5	1/2	21	4	2/3
			17	3	1/2	21.5	3.5	2/3
			17.5	2.5	1/2	22	3	2/3
			18	2	1/2	22.5	2.5	2/3
			18.5	1.5	1/2	23	2	2/3
			19	1	1/2	23.5	1.5	2/3
			19.5	0.5	1/2	24	1	2/3
						24.5	0.5	irrational

2.4.2 Chaotic Regions

There are two fundamentally different types of behaviour exhibited by the chaotic systems which can be seen using next return maps. There are some chaotic systems that display behaviour similar to a logistic map in that their next return maps are roughly parabolic.[8] An example from our model of a next return map with a parabolic shape is given in Figure 2.10a. There are also some chaotic systems that display behaviour similar to a sine map or circle map.[78] The sine map is of the form:

$$\theta_{i+1} = (\theta_i - k\sin(\theta_i) + \omega) \bmod 2\pi. \tag{2.7}$$

This map is illustrated in Figure 2.10c for $k = 3.5$ and $\omega = \frac{\pi}{2}$, a set of parameters at which this map displays chaos. An example, from our modified Tyson-Novak model, of a next return map with a similar shape to the sine map is given in Figure 2.10b.

There is also interesting behaviour when looking at the chaotic region in the parameter plane. The chaotic region consists of many islands as illustrated in Figure 2.11. There are large islands with long chains of small islands next to them. When all of these islands are looked at with more detail (Lyapunov exponents are calculated for smaller ranges of τ_{on} and τ_{off}) they are riddled with smaller and smaller non-chaotic regions. When the non-chaotic regions between the chains

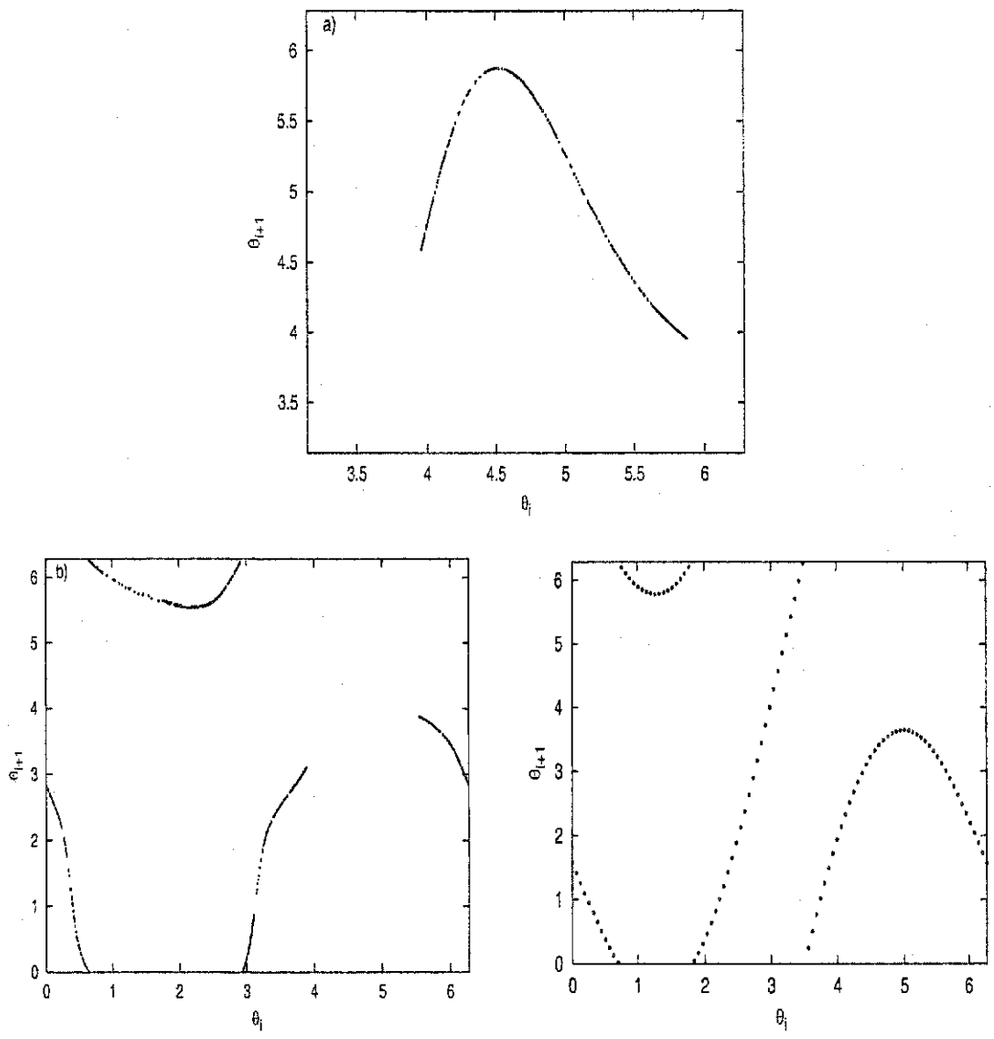

Figure 2.10: Different behaviours of chaotic systems: a) Next return map for $\tau_{on} = 24$ and $\tau_{off} = 6.75$ which resembles the parabolic shape of the logistic map. b) Next return map for $\tau_{on} = 7$ and $\tau_{off} = 2$ which resembles the sine map shape. c) Next return map of the sine map with $k = 3.5$ and $\omega = \frac{\pi}{2}$ which demonstrate chaotic behaviour.

of small islands of chaos are looked at in more detail, it is found that these non-chaotic regions are riddled with smaller regions of chaotic behaviour as well. This closer examination reveals a fractal nature of the chaotic region. A full examination of this fractal behaviour is discussed in Closson *et al.*[63] Fractal behaviour is also seen when looking at the Arnold tongues for the sine map[78] as well as in other systems.[3,79]

The chaotic region has some important biological implications. There are many physiological rhythms that behave irregularly.[16] For example, the opening and closing of channels in neurons[80,81] and cardiac cells that carry ionic current. Some irregular rhythms are due to noise (as in the above examples) and others are chaotic. Many models have been developed and experiments done describing the chaotic behaviour, as well as noise, in the cell division cycle.[20,40,82,83]

2.4.3 Routes to Chaos

In most cases the route to chaos observed between the periodic and chaotic regions in this system consists of period doubling bifurcations.[4,8] This route to chaos is also common in other externally forced systems.[2,20,72,84] Period doubling bifurcations can easily be illustrated by examining the winding numbers of the systems. As the name implies, the period, or in this case the winding number, doubles after

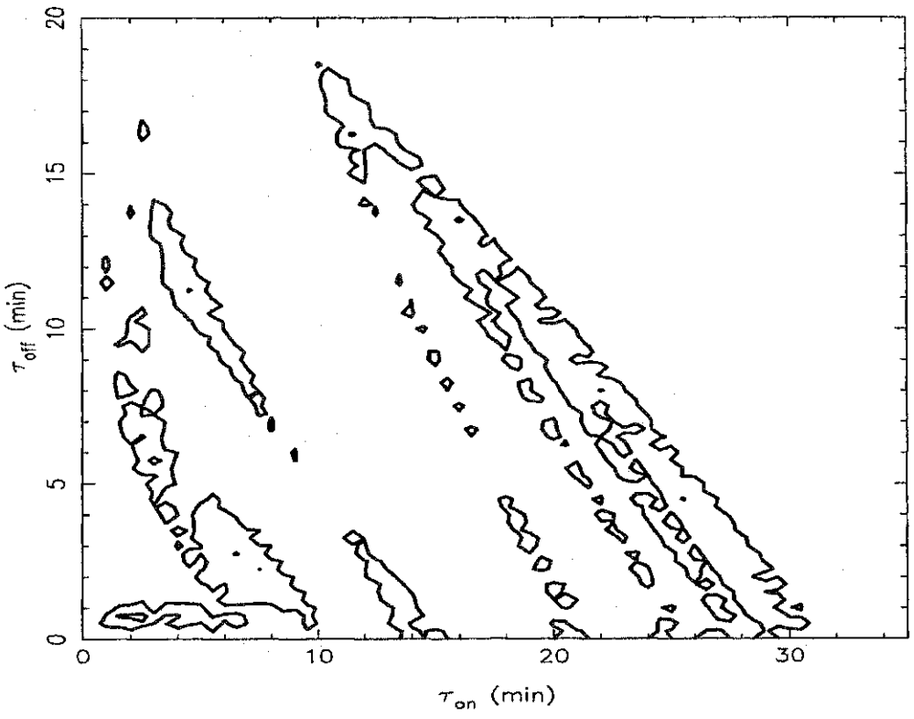

Figure 2.11: Chaotic regions or islands in the parameter plane calculated previously.[63] The resolution of this plot is 0.5 in the τ_{on} domain and the 0.25 in the τ_{off} range. When looked at with higher and higher resolution, the islands are riddled with regions of non-chaotic behaviour and non-chaotic regions between rows of islands of chaos are riddled with regions of chaos.

each bifurcation as the system progresses towards chaotic behaviour. For example, period doubling occurs between the chaotic region and the region where $\omega_a = \frac{1}{2}$. This is illustrated in a blown up section of the parameter plane in Figure 2.9b. The winding number doubles as the chaotic region is approached ($\frac{2}{4}$, $\frac{4}{8}$, $\frac{8}{16}$, etc.). It is difficult to resolve the regions of subsequent bifurcations after $\frac{4}{8}$ and especially after $\frac{8}{16}$ because the parameter range at which a given winding number is observed decreases with each bifurcation. As the number of bifurcations goes to infinity, the distances between subsequent bifurcations decrease so in this scenario, chaos results from an accumulation of period doublings. The Feigenbaum relationship describes this shrinking of the distance between successive bifurcations:

$$\delta = \lim_{n\to\infty} \frac{r_n - r_{n-1}}{r_{n+1} - r_n} = 4.669.... \tag{2.8}$$

where r_n denotes the parameter value at which the n^{th} period doubling bifurcation occurs. This relationship shows that the range of parameters in which the different locking ratios are observed decrease by a factor of about 4.669 with each bifurcation. Thus it is more difficult to resolve these smaller areas. The Feigenbaum relationship is a very common relationship to describe period doubling, however since the areas of doubling as $n \to \infty$ are difficult to resolve, it is difficult in this case to see this relationship. When looking at the peak pattern of these doubling regions, doubling also occurs in the peak pattern. For example, in another region

where period doubling occurs, the peak pattern S^2L changes to $(S^2L)^2$ after its first period doubling bifurcation. The original symbolic pattern just repeats itself. They are fundamentally the same pattern, except that the relative heights of each peak are different for the repeat of the original pattern in the doubled region. This is illustrated in Figure 2.12a-b. This doubling can also be illustrated by phase plane plots. When a system undergoes a period doubling bifurcation, the trajectory in the phase plane also doubles. In other words, for every orbit or loop in the original trajectory, two orbits or loops appear after the bifurcation. This is illustrated in Figure 2.12c-d.

The other less common route to chaos observed in this model is a saddle-node bifurcation of cycles, sometimes called a tangent bifurcation.[4,8] A tangent bifurcation is described as a stable cycle and an unstable cycle moving toward one another until they collide and mutually annihilate one another. When this occurs there is a noticeable stable limit cycle with certain parameters and then with a slight change in parameters the stable limit cycle disappears and chaos is the result. This type of almost instantaneous change from periodic to chaotic behaviour has also been observed in other models of biological systems.[8,16] However, closer investigation of the system is required to conclude that a tangent bifurcation has truly occurred. In this case the sudden appearance of chaos occurs in the parame-

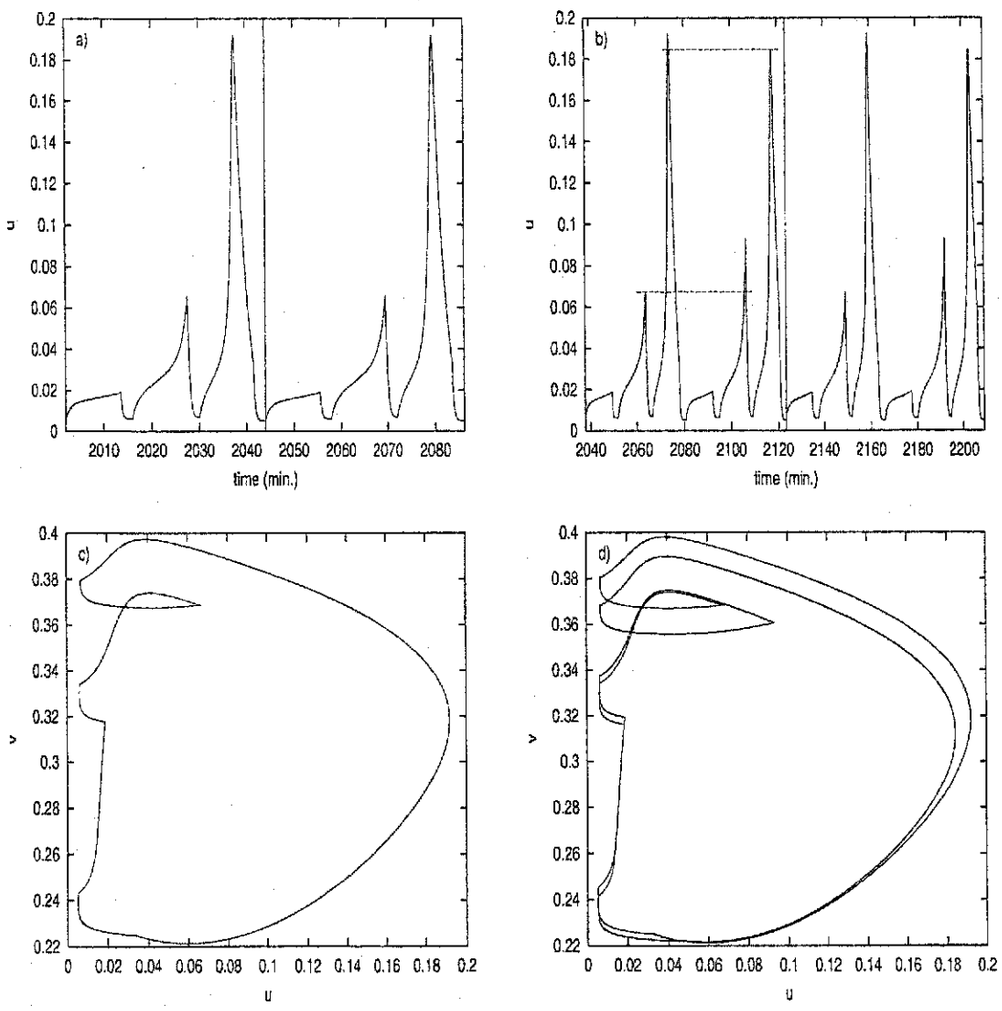

Figure 2.12: Period doubling examples: a) Time series plot with peak pattern of S^2L for the system $\tau_{on} = 11.5$ and $\tau_{off} = 2.5$. The vertical line separates the repeating unit. b) Time series plot with peak pattern of $(S^2L)^2$ for the system $\tau_{on} = 11.5$ and $\tau_{off} = 2.75$. The vertical line separates the repeating unit and the dashed horizontal lines show how the difference is only in the relative heights of the peaks. c) Phase plane plot with $\omega_a = \frac{1}{3}$ for the system $\tau_{on} = 11.5$ and $\tau_{off} = 2.5$. d) Phase plane plot with $\omega_a = \frac{2}{6}$ for the system $\tau_{on} = 11.5$ and $\tau_{off} = 2.75$.

ter plane in part of the area around the $\omega_a = \frac{1}{3}$ and $\omega_a = \frac{2}{3}$ regions. Both regions have $\omega_{all} = \frac{3}{3}$ so that there is an underlying period-3 behaviour. Tangent bifurcations of a period-3 orbit can be characterized by looking at the third power of the return map. If a tangent bifurcation has occurred the power-3 map will show one point on the diagonal for the periodic system and a spread of points nearly tangent to the diagonal just inside the chaotic region. The diagonal line in a power map will denote periodic behaviour. For example, in a power-3 map if the system is periodic with the number of driving periods for each repeat equal to 3, then every third point is the same, making that point fall on the diagonal line of the power map. The further into the chaotic region the system goes, the tangent area of the map should move away from the diagonal. This characteristic is illustrated in Figure 2.13 using power-3 maps. Another feature that goes along with tangent bifurcations is called intermittency. Intermittency is a chaotic system that looks nearly periodic for a length of time, then looks chaotic for a short length of time and then looks nearly periodic again. These intermittent complex bursts occur irregularly between the apparently periodic sections making the overall system chaotic. Intermittency occurs close to the tangent bifurcation and as the tangent moves further from the diagonal of the power maps the intermittent chaos occurs more frequently and for longer durations until the system appears chaotic every-

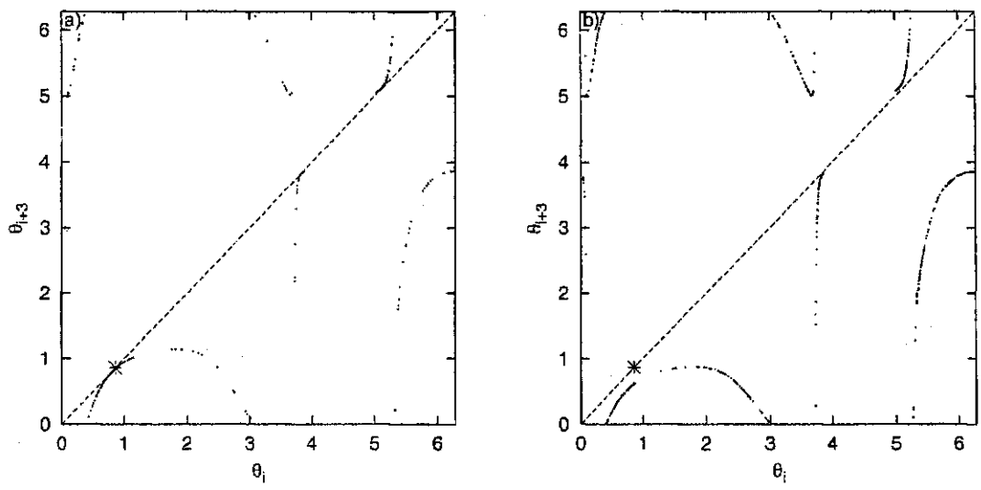

Figure 2.13: Tangent bifurcation examples using systems with $\omega_a = \frac{1}{3}$ and the chaotic region nearby: a) Power-3 map of the chaotic system with $\tau_{on} = 6.5$ and $\tau_{off} = 8.3$ as the small points. The dashed line represents the diagonal and the star ($*$) represents a point from the periodic system with $\tau_{on} = 6.5$ and $\tau_{off} = 8.29$. There are three places on this plot where the chaotic system is very close to being tangent to the diagonal. These tangencies correspond to the three fixed points of the period-3 map below the bifurcation value of τ_{off}. b) Power-3 map of the chaotic system with $\tau_{on} = 6.5$ and $\tau_{off} = 8.5$ as the small points. The dashed line represents the diagonal and the star represents a point from the periodic system with $\tau_{on} = 6.5$ and $\tau_{off} = 8.29$. Note that the three tangencies are moving away from the diagonal.

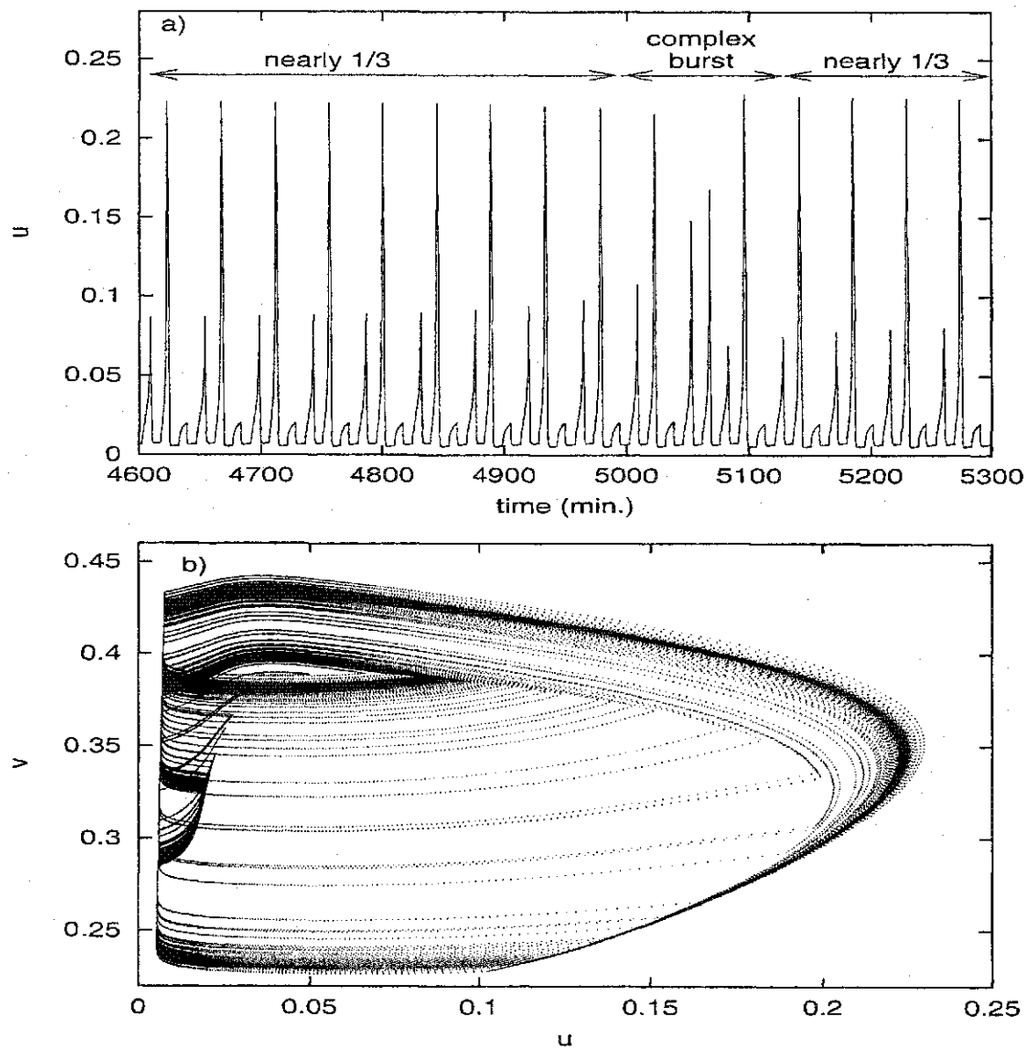

Figure 2.14: Examples of intermittent behaviour for the chaotic system with $\tau_{on} = 6.5$ and $\tau_{off} = 8.3$ with a nearly $\frac{1}{3}$ winding number behaviour: a) Times series plot and b) strange attractor.

where with no bits of periodic behaviour. This characteristic of intermittency is illustrated in Figure 2.14 using a time series plot and a phase plane plot of the chaotic attractor, which is often referred to as a strange attractor. From this evidence we conclude that the other route to chaos that occurs is a tangent bifurcation or a saddle-node bifurcation of cycles.

2.4.4 Multiples of the Natural Period

In the Tyson-Novak model the natural period, T_{NT}, of the oscillator ($k_{\text{wee}} = 1.5$) is approximately 34.35 minutes. Since the value of τ_{on} represents the oscillating dynamics it is of interest to see if the system exhibits a pattern of behaviour for values of τ_{on} plus multiples of the natural period. To look for a pattern, τ_{off} is held constant with a value of 3.5 and $\tau_{\text{on}} = \tau_{\text{on}}^{\text{ref}} + nT_{NT}$. The results of different peak patterns and ω_a's for multiples of the natural period are given in Table 2.3. From this Table we see that the values ω_a follow a pattern of:

$$\omega_a(\tau_{\text{on}}^{\text{ref}} + nT_{NT}, \tau_{\text{off}}) = \frac{r + np}{p}, \tag{2.9}$$

where n is an integer representing the multiple of the natural period, r is the number of responses above the threshold when $n = 0$ and p is the number of driving periods for a repeating unit of the pattern. In other words, for every multiple of the natural period, n, the system gains a response above the threshold for every

Table 2.3: Pattern and ω_a for multiples of natural period, where n is an integer representing the multiple of the period, nT_{NT}, $\tau_{on} = \tau_{on}^{ref} + nT_{NT}$ and $\tau_{off} = 3.5$.

τ_{on}^{ref}	n = 0		n = 1		n = 2		n = 3	
	pattern	ω_a	pattern	ω_a	pattern	ω_a	pattern	ω_a
0	—	—	SL	1/1	SL^2	2/1	SL^3	3/1
1	S	0/1	SL	1/1	SL^2	2/1	SL^3	3/1
2	S	0/1	SL	1/1	SL^2	2/1	SL^3	3/1
3	S	0/1	SL	1/1	SL^2	2/1	SL^3	3/1
4	chaotic	—	SL	1/1	SL^2	2/1	SL^3	3/1
5	$(S^2L)^5$	5/15	SL	1/1	SL^2	2/1	SL^3	3/1
6	chaotic	—	SL	1/1	SL^2	2/1	SL^3	3/1
7	chaotic	—	chaotic	—	chaotic	—	$(SL^7)^8$	56/16
8	$(S^2L)^2$	2/6	$(SL)^2L^2$	4/3	$(SL^2)^2L^3$	7/3	$(SL^3)^2L^4$	10/3
9	S^2L	1/3	$(SL)^2L^2$	4/3	$(SL^2)^2L^3$	7/3	$(SL^3)^2L^4$	10/3
10	S^2L	1/3	$(SL)^2L^2$	4/3	$(SL^2)^2L^3$	7/3	$(SL^3)^2L^4$	10/3
11	S^2L	1/3	$(SL)^2L^2$	4/3	$(SL^2)^2L^3$	7/3	$(SL^3)^2L^4$	10/3
12	chaotic	-	chaotic	—	$(SL^5)^4$	20/8	$(SL^6)^4$	28/8
13	SL	1/2	SL^3	3/2	SL^5	5/2	SL^7	7/2
14	SL	1/2	SL^3	3/2	SL^5	5/2	SL^7	7/2
15	SL	1/2	SL^3	3/2	SL^5	5/2	SL^7	7/2
16	S^2L	1/2	SL^3	3/2	SL^5	5/2	SL^7	7/2
17	S^2L	1/2	$(SL)^2L$	3/2	$(SL^2)^2L$	5/2	$(SL^3)^2L$	7/2
18	S^2L	1/2	$(SL)^2L$	3/2	$(SL^2)^2L$	5/2	$(SL^3)^2L$	7/2
19	chaotic	—	chaotic	—	chaotic	—	$SL^4SL^8SL^3SL^4SL^{11}$	30/8
20	$(SL)^2$	2/3	$(SL^2)^2L$	5/3	$(SL^3)^2L^2$	8/3	$(SL^4)^2L^3$	11/3
21	$(SL)^2$	2/3	$(SL^2)^2L$	5/3	$(SL^3)^2L^2$	8/3	$(SL^4)^2L^3$	11/3
22	$(SL)^2$	2/3	$(SL^2)^2L$	5/3	$(SL^3)^2L^2$	8/3	$(SL^4)^2L^3$	11/3
23	$(SL)^2L^2$	4/5	chaotic	—	chaotic	—	$SL^7SL^4SL^{12}$	23/6
24	$(SL)^3$	3/4	$(SL^2)^3L$	7/4	$(SL^3)^3L^2$	11/4	$(SL^4)^3L^3$	15/4
25	chaotic	—	$(SL^2)^3L^4SL^3$	13/7	chaotic	—	$(SL^4)^2L^3(SL^4)^2SL^{12}$	31/8
26	$(SL)^4$	4/5	$(SL^2)^4L$	9/5	$(SL^3)^4L^2$	14/5	$SL^4)^3L^7$	19/5
27	chaotic	—	chaotic	—	chaotic	—	chaotic	—
28	chaotic	—	L^6	6/3	?	?	chaotic	—
29	L^2	2/2	L^4	4/2	L^6	6/2	L^8	8/2
30	L	1/1	L^2	2/1	L^3	3/1	L^4	4/1
31	L	1/1	L^2	2/1	L^3	3/1	L^4	4/1
32	SL	1/1	SL^2	2/1	SL^3	3/1	SL^4	4/1
33	SL	1/1	SL^2	2/1	SL^3	3/1	SL^4	4/1
34	SL	1/1	SL^2	2/1	SL^3	3/1	SL^4	4/1

driving period in that repeating unit. This can be seen by looking at the peak patterns. If a system has 3 driving periods per repeat, then the next multiple of the natural period has 3 more large (L) peaks in its peak pattern. An example of the similarities between the different multiples of the natural period is given using phase plane plots in Figure 2.15. As τ_{on} is increased by its natural period the system moves toward and then continues around the basic limit cycle for $k_{wee} = 1.5$ until the switch is again turned off. Therefore the trajectories for all the multiples look almost identical. There are slight differences near the points where the system undergoes a switching of the k_{wee}, and this is due to a slight difference in the time it takes to move between the stable point when $k_{wee} = 3.5$ and the limit cycle. The pattern follows for most cases except for a few special cases when $\tau_{on}^{ref} = 23, 25, 28$. These cases are situated very near a periodic-chaotic boundary. Since there are slight differences due to the transition between $k_{wee} = 1.5$ and $k_{wee} = 3.5$, the system will fall either in the periodic regime or in the chaotic regime.

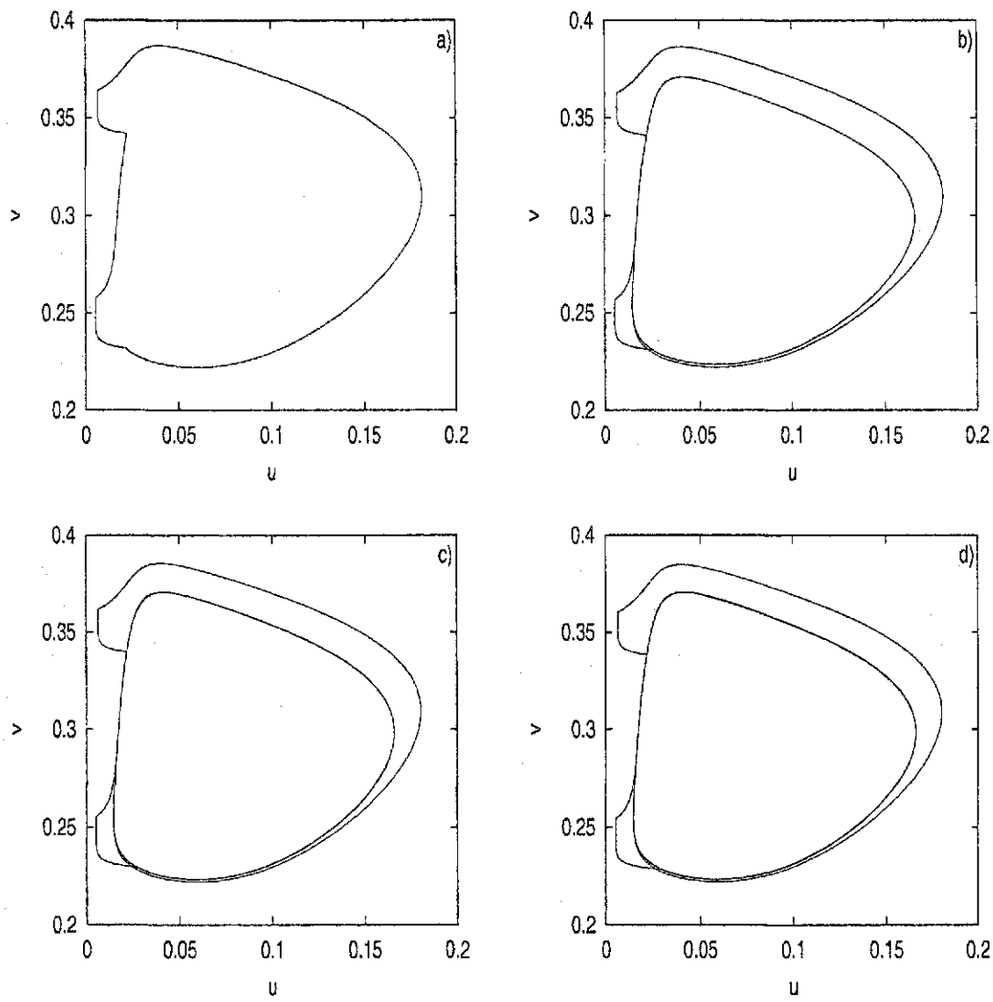

Figure 2.15: Phase plane plots for different multiples of $\tau_{on}^{ref} = 14$ with $\tau_{off} = 3.5$. Plots show the similarity between the systems as each system increases by its natural period. They all move towards and then continue around the basic limit cycle for $k_{wee} = 1.5$ until the switch is again turned off. a) Phase plane plot with $\omega_a = \frac{1}{2}$ for the system $\tau_{on} = 14$. b) Phase plane plot with $\omega_a = \frac{3}{2}$ for the system $\tau_{on} = 48.35$. c) Phase plane plot with $\omega_a = \frac{5}{2}$ for the system $\tau_{on} = 82.7$. d) Phase plane plot with $\omega_a = \frac{7}{2}$ for the system $\tau_{on} = 117.05$.

Chapter 3

Leaf Vein Formation Model

3.1 Auxin and Leaf Vein Formation

A basic schematic of different plant parts is given in Figure 3.1. The different rhythms in plants are an important focus of study.[13] The mechanisms for plant growth and cell differentiation are complex and have also been the focus of study for some time. One hormone in particular has been singled out as being involved in numerous different areas and stages of cell growth and cell differentiation in plants.[86] This hormone is auxin, or indole-3-acetic acid (IAA). Molecular structures of naturally occurring auxins are given in Figure 3.2. It is believed that auxin is synthesized from tryptophan, or indole, primarily in leaf primordia, young leaves and in developing seeds.[87] This hormone has been linked to cell enlargement,[88] cell division,[89,90] vascular tissue differentiation,[89] root initiation,[90] tropistic (bending) responses to light and gravity,[91,92] fruit setting and growth,[93]

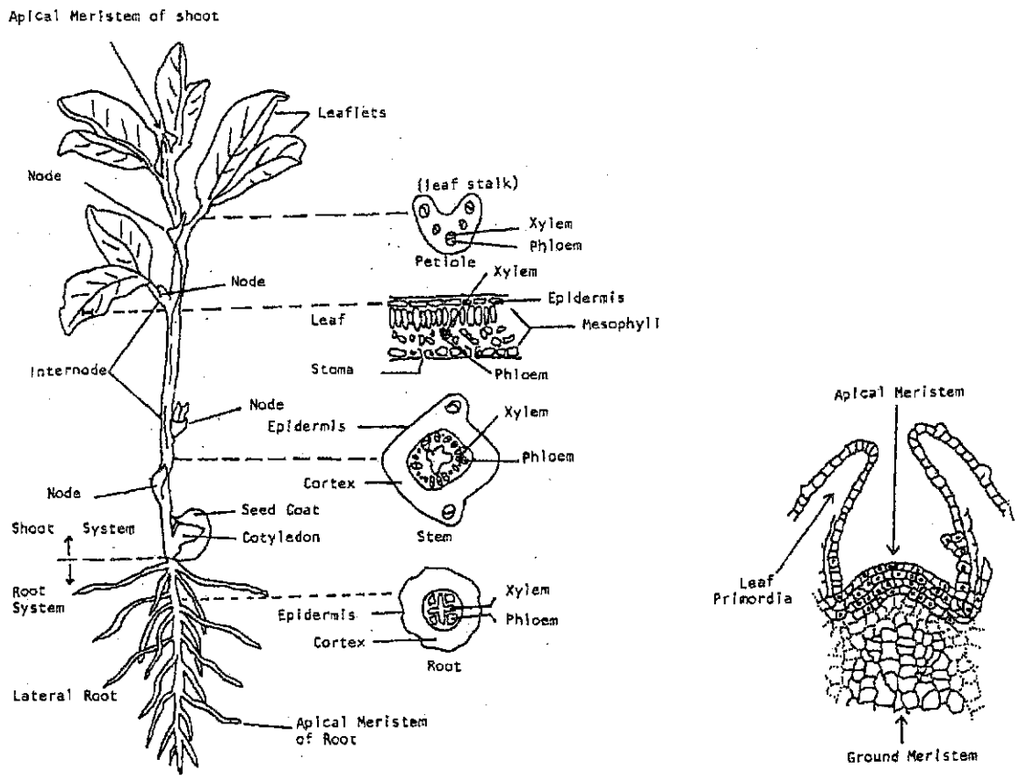

Figure 3.1: Schematic of different plant parts. The full plant on the left is a representation of a broad bean, *Vicia faba* plant. The close up on the right of the apical meristem is a representation of a common dicot house plant, *Coleus blumei* Adapted from Raven *et al.*[85]

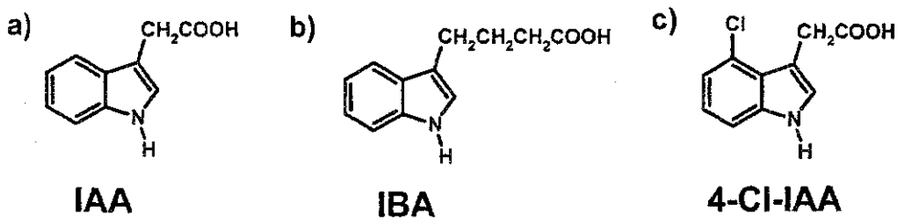

Figure 3.2: Molecular structures of auxin and other analogs.[86] a) The most common naturally occurring form of auxin, indole-3-acetic acid (IAA). b) Another naturally occurring form of auxin, indole-3-butyric acid (IBA). c) A halogenated naturally occurring form of auxin, 4-chloroindole-3-acetic acid (4-Cl-IAA).

flowering[94] and much more. Auxin was first theorized by Darwin in 1880[95] and was first captured in agar by Went in 1926.[96] Auxin in its IAA form was first isolated and purified by Haagen-Smit *et al.* in 1946.[97] Since vein formation in leaves is the focus of our model, a hypothesis formulated about auxin in connection with the differentiation of vein formation in leaves is the focus here. A hypothesis by Sachs for the differentiation of leaf vein formation in relation to auxin is summarized below.[98,99]

In his hypothesis, Sachs refers to auxin as a differentiation-inducing signal. He states that interactions between cells in the differentiating tissue are due to differences in the rate and axis of transport of a differentiation-inducing signal. Cells that transport more of this signal along a certain axis promote the differentiation of other cells along the same column of cells and inhibit the same differentiation in other directions, from which the signal is drained. Therefore, cells limit or

promote differentiation to defined stands by temporal changes in the cells themselves. For example, if there is enough auxin in a cell to promote differentiation, the change that occurs within the cell promotes increased auxin transport. The change causes an autocatalytic increase in the rate, or capacity, of the signal to move along the axis it was previously moving. The initial movement is thought to be caused by a concentration gradient. Therefore, the same signal (auxin) may be used for both long range correlations and for the interaction of neighbouring cells. An example of experimental evidence for the autocatalytic increase in rate for the movement of signal was provided by Sachs in 1975.[100] He measured the transport of radioactive auxin at various times through a region where a future strand appeared. Auxin transport increased in this area before differentiation of the vein could be observed. This showed that early stages of vascular differentiation are associated with an increase in transport of auxin.

3.2 The Model

There is a simple mathematical model describing the movement of auxin in a two-dimensional array of square cells proposed by Mitchison[101] which explains some aspects of vein formation in higher plants. Mitchison makes some simplifying assumptions that a leaf is two-dimensional and that each cell is square. Some as-

sumptions are also made in regard to auxin's movement and influence based on some of Sachs's results. This model consists of 2N differential equations along with some relationships between auxin concentration (s), the diffusion coefficient (D) and flux (ϕ). In this model, the auxin concentration in most cells is dependent only on the flux of auxin coming into or out of the cell. In a vein, auxin is transported away quickly. Since auxin can be transported away much more quickly than it can diffuse in, the auxin concentration in these cells is negligible and they act as auxin sinks. There are also certain cells which produce auxin. It is assumed that auxin moves through and between cells by diffusion. Since diffusion through membranes is much slower than diffusion within a cell, each cell can be treated as a well-mixed compartment. The flux across a cell membrane (ϕ) is defined as being proportional to the difference of auxin concentration between two cells. Each cell has a set of differential equations for s and D defined on a square matrix (m,n) of cells. The organization of these variables on the matrix is given in Figure 3.3. The arrangement of having a sink or vein on one side of the matrix and a source on the other is chosen because this arrangement often occurs in a leaf. Auxin is produced in cells along the edge of the leaf (represented by the rightmost column of the matrix). In the center of the leaf is the mid-vein (represented by the leftmost column). The mid-vein is separated from the auxin-producing cells by a number

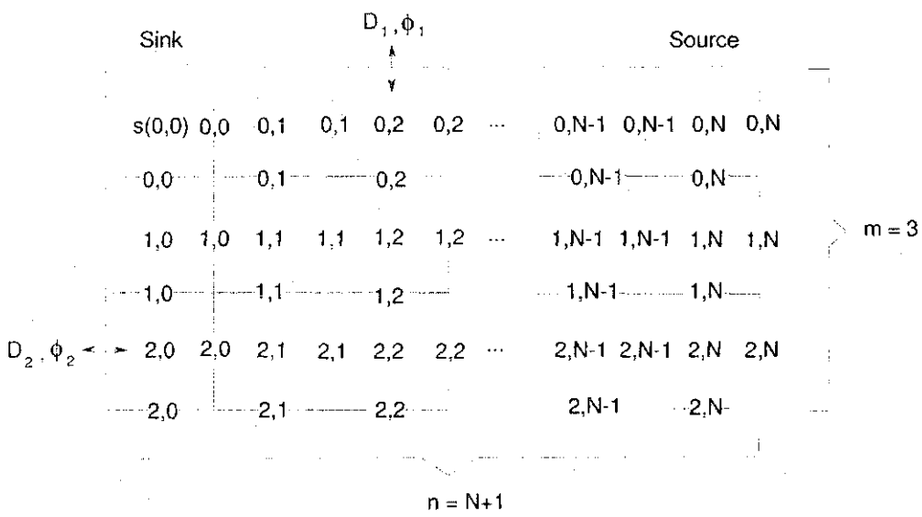

Figure 3.3: Schematic of matrix for vein formation with a line source of auxin production and a sink. The numbering convention shown here is used in our model. The fluxes (ϕ) and diffusion coefficients (D) along the bottom and right edge of the matrix are constrained to be zero. This makes all the edges have the same boundary condition.

of columns of ordinary cells which do not produce auxin. It is of interest to see how new veins will form in this simplified situation.

The diffusion coefficients and flux variables are divided into two groups. The flux and diffusion coefficient between cells in a column are symbolized by D_1 and ϕ_1. The flux and diffusion coefficient between cells in a row are symbolized by D_2 and ϕ_2. The sign of the flux for both columns and rows indicates the direction of net flow. The numbering convention adopted means that, for example, if the flux $\phi_1(1,1)$ is negative, then auxin moves from cell (1,1) (higher auxin concentration) to cell (2,1) (lower auxin concentration).

The equations for each cell are given below.

$$s(m,0) = 0 \tag{3.1}$$

This is the sink condition: A major vein is assumed to transport auxin away so efficiently that its concentration is effectively zero.

$$\phi_{\text{net}} = \phi_1(m,n) - \phi_1(m-1,n) + \phi_2(m,n) - \phi_2(m,n-1) \tag{3.2}$$

This equation expresses the net flux that a cell (m,n) experiences. The sign of the second and fourth terms are needed because of the way direction is assigned for flux. Boundary cells have a modified equation from Equation 3.2 with one or two less terms depending on their position in the matrix. (The flux is zero across the

top and left edges.)

$$\frac{ds(m,N)}{dt} = \sigma + \phi_{net} \tag{3.3}$$

Equation 3.3 describes the change in auxin concentration with time at the source, with σ being an auxin production term.

$$\frac{ds(m,n)}{dt} = \phi_{net} \tag{3.4}$$

This equation describes the change in auxin concentration with time for all the cells between the source and sink.

$$\phi_1 = D_1(m,n)[s(m+1,n) - s(m,n)] \tag{3.5}$$

$$\phi_2 = D_2(m,n)[s(m,n+1) - s(m,n)] \tag{3.6}$$

These are the equations for flux with the subscript 1 for flux perpendicular to the source-sink direction and the subscript 2 for the flux in the source-sink direction.

$$\frac{dD_i(m,n)}{dt} = f[|\phi_i(m,n)|] - \gamma D_i, (i = 1,2) \tag{3.7}$$

Equation 3.7 expresses the change in the diffusion coefficient with time described by a production and a destruction term. The first term is the production term expressed as a function f. The second term is the destruction term, where the diffusion coefficient decreases at a specific rate γ. The subscript i describes the

direction as for the flux.

$$f(|\phi_i|) = \frac{\alpha\delta^{\eta}(\frac{\phi_i}{\delta})^{\eta}}{1+(\frac{\phi_i}{\delta})^{\eta}} + \beta \tag{3.8}$$

The function f is the change in production of the diffusion coefficient with time. In the absence of flux, $f \rightarrow \beta$ and therefore $D_i \rightarrow \frac{\beta}{\gamma}$. The first term in f allows D_i to increase in response to flux ϕ_i. Mitchison required this function to have an upper and lower bound limit. The function Mitchison used had a specific shape. We chose our function to be similar to Mitchison's function with a slightly different form. With our form we could manipulate the steepness of the Hill function[102] by changing η. The values D_i and ϕ_i that border the bottom and right edge of the two-dimensional array of cells are given a value of zero for all time. These boundaries are similar to the edge of a leaf, in that auxin cannot flow outside of the leaf. The size of our matrix is the same as the size Mitchison used. He used a 10x8 matrix. This number of cells is likely much smaller than an actual leaf at a stage of early development. However, for simplicity we chose the same size.

3.3 Computer Simulations and Data Collection

3.3.1 Periodic Driving

A high-low switch for σ is implemented in the same manner as the on-off switch described on page 15. The parameters t_h and t_l correspond to the time the switch spends at the assigned high or low value. These values of high and low auxin production are represented by the variables σ_h and σ_l, respectively. In this system the weighted average of these variables is important in defining the behaviour. The weighted average is calculated as:

$$\bar{\sigma} = \frac{\sigma_h t_h + \sigma_l t_l}{t_h + t_l} \tag{3.9}$$

3.3.2 Time Series Data

We are interested in the evolution of flux, ϕ, in time. We look at two different systems. A system with a line source is described above in Figure 3.3. We also study a system with a point source where only one cell on the right hand side of the matrix has a production (σ) term. Most of the focus will be on the line source system unless otherwise stated.

There are two basic types of possible behaviours. There can be vein formation, which is characterized by a large increase of flux in one or more rows in the

direction between the source and sink with rows of reduced flux to either side. The other type of behaviour is no-vein formation, which is characterized by a flux field which is either completely homogeneous or, at minimum, homogeneous in the direction perpendicular to the source-sink axis. For both types of no-vein behaviour the fluxes between cells in the direction perpendicular to the source-sink axis are zero. For the completely homogeneous system the fluxes between the source and sink are all constant and for the other type of system the flux between the cells in the source and sink direction are slightly decreasing from source to sink with each column of flux from source to sink being constant. The non-homogeneous no-vein behaviour has $\phi_1(m,n) = 0$ and $\phi_2(m,1) = X_1$, $\phi_2(m,2) = X_2$, $\phi_2(m,3) = X_3$, with $X_1 > X_2 > X_3$ and so on. Since the value of ϕ_1 is zero across all cell membranes for no-vein behaviour, it is useful to only look at ϕ_2. Examples of the ϕ_2 matrices for all the types of behaviour are given in Figure 3.4. In each case, the matrices represent stationary behaviour after the transients have decayed.

The systems without switching can exhibit vein formation (including multiple veins) and homogeneous no-vein behaviour. The systems with switching can exhibit vein formation (including multiple veins) and non-homogeneous no-vein behaviour. The two show different no-vein behaviour because when the production term (σ) is constant, the system stabilizes and becomes homogeneous. However,

a)

5.166023	5.075252	4.848151	4.413492	3.706216	2.699312	1.428002	0.000000
5.166023	5.075252	4.848151	4.413492	3.706216	2.699312	1.428002	0.000000
5.166023	5.075252	4.848151	4.413492	3.706216	2.699312	1.428002	0.000000
5.166023	5.075252	4.848151	4.413492	3.706216	2.699312	1.428002	0.000000
5.166023	5.075252	4.848151	4.413492	3.706216	2.699312	1.428002	0.000000
5.166023	5.075252	4.848151	4.413492	3.706216	2.699312	1.428002	0.000000
5.166023	5.075252	4.848151	4.413492	3.706216	2.699312	1.428002	0.000000
5.166023	5.075252	4.848151	4.413492	3.706216	2.699312	1.428002	0.000000
5.166023	5.075252	4.848151	4.413492	3.706216	2.699312	1.428002	0.000000
5.166023	5.075252	4.848151	4.413492	3.706216	2.699312	1.428002	0.000000

b)

5.420474	5.460616	5.580404	5.895262	6.696537	8.660412	12.988623	0.000000
55.716626	55.590774	55.225533	54.323773	52.236437	47.659742	38.324397	0.000000
5.499305	5.586020	5.797018	6.212510	6.954786	8.218986	10.857814	0.000000
5.520115	5.656765	6.007718	6.772112	8.364372	11.440723	16.038365	0.000000
5.378455	5.471475	5.709357	6.221396	7.274360	9.390632	13.490810	0.000000
50.136107	49.883186	49.287911	48.117977	45.863793	41.495363	33.334410	0.000000
5.200873	5.199213	5.206864	5.269046	5.551782	6.628071	10.284042	0.000000
53.651652	53.460780	52.991034	52.034899	50.187972	46.565321	39.772673	0.000000
5.601016	5.694999	5.905247	6.270150	6.824340	7.606880	9.078756	0.000000
5.820006	5.996733	6.416508	7.237339	8.756753	11.424852	15.517885	0.000000

c)

7.095532	7.284764	7.696463	8.390995	9.430214	10.811617	12.395834	0.000000
6.815649	6.946245	7.235999	7.748864	8.597628	9.940911	11.849546	0.000000
6.369758	6.407047	6.497773	6.687716	7.096091	8.028019	10.129519	0.000000
64.500415	63.554396	61.536486	58.168267	52.955971	45.074004	33.203182	0.000000
6.689727	6.685318	6.686416	6.720272	6.853819	7.261348	8.488993	0.000000
7.597754	7.655500	7.791361	8.055989	8.556345	9.508993	11.283827	0.000000
8.602366	8.714709	8.962925	9.398270	10.101468	11.154980	12.532240	0.000000
9.672877	9.817824	10.122096	10.608575	11.290410	12.138308	13.057182	0.000000
10.770715	10.914269	11.199224	11.616295	12.141828	12.737376	13.364349	0.000000
11.885207	12.019928	12.271257	12.604756	12.976225	13.344443	13.685328	0.000000

d)

10.000000	10.000000	10.000000	10.000000	10.000000	10.000000	10.000000	0.000000
10.000000	10.000000	10.000000	10.000000	10.000000	10.000000	10.000000	0.000000
10.000000	10.000000	10.000000	10.000000	10.000000	10.000000	10.000000	0.000000
10.000000	10.000000	10.000000	10.000000	10.000000	10.000000	10.000000	0.000000
10.000000	10.000000	10.000000	10.000000	10.000000	10.000000	10.000000	0.000000
10.000000	10.000000	10.000000	10.000000	10.000000	10.000000	10.000000	0.000000
10.000000	10.000000	10.000000	10.000000	10.000000	10.000000	10.000000	0.000000
10.000000	10.000000	10.000000	10.000000	10.000000	10.000000	10.000000	0.000000
10.000000	10.000000	10.000000	10.000000	10.000000	10.000000	10.000000	0.000000
10.000000	10.000000	10.000000	10.000000	10.000000	10.000000	10.000000	0.000000

flux into sink — $\phi_2(8,2)$ — flux out of source — leaf edge no flux

Figure 3.4: Examples of different behaviours of ϕ_2 with the sink on the left and the source on the right. a) No vein formation of a non-homogeneous system with $\sigma_h = 10$, $\sigma_l = 0$, $t_h = 50$, $t_l = 50$ and $\bar{\sigma} = 5$. b) Formation of three veins with $\sigma_h = 20$, $\sigma_l = 10$, $t_h = 50$, $t_l = 1$ and $\bar{\sigma} \approx 19.8$. c) Formation of one vein with a constant $\sigma = 14$. d) No vein formation of a homogeneous system with a constant $\sigma = 10$.

when the production term (σ) is changed periodically, the system can stabilize but since σ is constantly changing over time the system can not be homogeneous. A way to characterize the vein formation behaviour is to count the number of veins formed and also to calculate how fast the veins are formed. If a system is going to have multiple veins, they all appear at the same time. Therefore, there is only one vein formation time to consider.

To calculate the type of data in which we are interested, a computer simulation program was developed. An explicit Euler method[71] is used to integrate the differential equations of our modified Mitchison model.* The stepsize (h) for the explicit Euler method is a user-defined parameter. For the unswitched systems σ is a user-defined parameter. For the switched systems different values of σ_h, σ_l, t_h and t_l are user-defined parameters. The system is started with the initial values of $\phi_i(0) = 0$, $D_1(0) = 0.1625$, $D_2(0) = 0.325$, and the $s(m,n)$ are each given a random initial value between 0 and 10, except for the case $n = 0$ which represents the sink and has a value of zero for all time. The random number generator used is an implementation of those discussed in Marsaglia and Zaman.[103] In most simulations the same seed was used, to allow reproducibility of the computational results. However, in some cases a different seed was used to study the sensitivity

*The Euler method was chosen for its simplicity, since other more complicated integrators gave the same results.

to initial conditions.

The values of some of the parameters in this model were needed so an investigation into the range of parameters that gave similar behaviour to Mitchison's results was carried out. The unswitched system was first studied to determine interesting values of the parameters. Most parameters gave Mitchison's vein formation results for a range of values. A value was then picked from this range to be approximately the average value or the smallest value required. For example, η gave vein formation results for values ranging from 3 to 6. As η increases, the steepness of the Hill function increases slightly. Since increasing η gave basically the same results for vein formation, we chose the smallest, simplest value, $\eta = 3$ for the Hill function. For δ, a range of values that gave vein formation results was from 52-20, the value $\delta = 35$ is about the average of the range. The initial values for D_1 and D_2 also could be given a range of starting values to get vein formation results. However, these values were chosen to be the same as Mitchison's initial values for these parameters. The values of the parameters used in this study are given in Table 3.1.

Next, we studied the behaviour of the system for a range of σ. In particular, we measured the time it takes for vein formation to occur. The criteria for vein formation were derived from the matrix for ϕ_2: A vein was recognized when

Table 3.1: Vein Parameter Table

Parameter	α	β	γ	δ	η	$D_1(t=0)$	$D_2(t=0)$
Value	1.429e-6	5e-3	5e-2	35	3	0.1625	0.325

neighbouring values perpendicular to the source-sink direction were at least some multiple of one another. We found that it was only necessary to look at the first two columns of the ϕ_2 matrix next to the sink and compare each neighbour in the perpendicular direction. If any of the fluxes were three times larger than their neighbours, vein formation was considered complete. Within reason, the multiple chosen didn't matter, however three was chosen as the lowest multiple that gave consistent results. The columns closest to the sink were used because the difference in flux between rows was the most pronounced there. This can be seen by looking at the two examples of vein formation in the ϕ_2 matrices in Figure 3.4.

Lastly, we determined the behaviour of the switched system for a range of σ_h, σ_l, t_h and t_l, including the time it took for vein formation to occur.

3.4 Results

3.4.1 Point Source System

The behaviour of both the unswitched and the switched systems with a point source is quite simple. When looking at the unswitched systems, if the auxin production term σ is small, a vein will not form. In this case, the auxin is being removed by diffusion too quickly. As the production term is increased, a weak vein appears. A weak vein has high flux near the source and the flux diminishes toward background values as it moves towards the sink. As σ is increased further, a single vein forms, then a double vein, then a triple vein and so on. As σ increases, the width of the vein increases. Examples of the different widths of veins are illustrated with ϕ_2 matrices in Figure 3.5.

The switched system gives similar results with two slight variations. The first is that a vein can form faster for the switched system. This occurs for instance when $\bar{\sigma} = 55$ or 60 (Table 3.2). For the rest of the systems compared, they all formed veins at the same time. The other variation occurs in the transition from one to two width of vein and two to three width of vein. This transition occurs sooner or with a smaller $\bar{\sigma}$ value for the switched systems. Both of these variations in results are illustrated in Table 3.2.

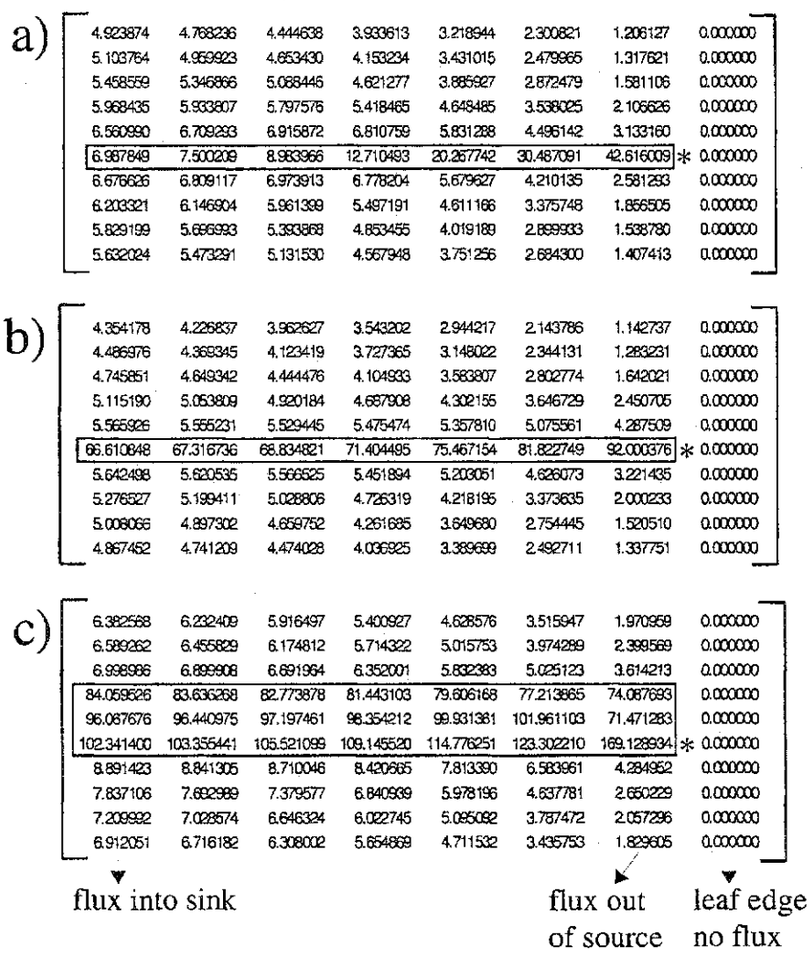

Figure 3.5: Examples of different behaviour of flux for unswitched point source systems. The star ($*$) represents the place where the point source is located. a) A weak vein for a system with $\sigma = 50$. b) One vein for a system with $\sigma = 100$. c) Triple vein for a system with $\sigma = 180$.

Table 3.2: Behaviour for a range of unswitched and switched point source systems. The section separated by horizontal lines show where the width of the vein changes differently between the switched and unswitched systems. The time required for vein formation is given by t.

No Switch			Switch, $t_h = 10\, t_l = 10$				
σ	# of veins	t	σ_h	σ_l	$\bar{\sigma}$	# of veins	t
50	1 weak vein	10000+	100	0	50	1 weak vein	10000+
55	1 weak vein	10000+	110	0	55	1 vein	708.36
60	1 vein	714.92	120	0	60	1 vein	500.01
65	1 vein	500.01	130	0	65	1 vein	500.01
70	1 vein	500.01	140	0	70	1 vein	500.01
75	1 vein	500.01	150	0	75	1 vein	500.01
80	1 vein	500.01	160	0	80	1 vein	500.01
85	1 vein	500.01	170	0	85	1 vein	500.01
90	1 vein	500.01	180	0	90	1 vein	500.01
95	1 vein	500.01	190	0	95	1 vein	500.01
100	1 vein	500.01	200	0	100	1 vein	500.01
105	1 vein	500.01	210	0	105	2 vein	500.01
110	1 vein	500.01	220	0	110	2 vein	500.01
115	1 vein	500.01	230	0	115	2 vein	500.01
120	2 vein	500.01	240	0	120	2 vein	500.01
125	2 vein	500.01	250	0	125	2 vein	500.01
130	2 vein	500.01	260	0	130	2 vein	500.01
135	2 vein	500.01	270	0	135	2 vein	500.01
140	2 vein	500.01	280	0	140	2 vein	500.01
145	2 vein	500.01	290	0	145	2 vein	500.01
150	2 vein	500.01	300	0	150	2 vein	500.01
155	2 vein	500.01	310	0	155	2 vein	500.01
160	2 vein	500.01	320	0	160	2 vein	500.01
165	2 vein	500.01	330	0	165	3 vein	500.01
170	3 vein	500.01	340	0	170	3 vein	500.01
175	3 vein	500.01	350	0	175	3 vein	500.01
180	3 vein	500.01	360	0	180	3 vein	500.01
185	3 vein	500.01	370	0	185	3 vein	500.01
190	3 vein	500.01	380	0	190	3 vein	500.01
195	3 vein	500.01	390	0	195	3 vein	500.01
200	3 vein	500.01	400	0	200	3 vein	500.01

Table 3.3: Range of σ for different vein numbers.

Number of Veins	1	2	3	4	5	6	7
Range of σ	13-14	15-18	19-21	22-27	28-32	33-35	36-38

The reason for the similarity in time for vein formation in most of these results is unclear.

3.4.2 Line Source System

For vein formation to occur in the unswitched line source systems, σ has to fall within a range. Below this range, the production of auxin is insufficient to produce vein patterns and a homogeneous veinless pattern develops. Above this range, the production of auxin is so large that it swamps the matrix of cells with so much auxin that vein differentiation cannot occur and a homogeneous veinless pattern develops. Between these two thresholds a vein or a number of separate single veins form. An example of a three vein system is given in Figure 3.4b. This example is for a switched system, however the resulting ϕ_2 matrices for both the switched and unswitched cases look similar at the same mean value of σ. The range in which vein behaviour is observed is $\sigma = 13$ to 38. The different ranges for different numbers of veins is given in Table 3.3. When the vein pattern reaches

5 out of only 10 rows, then double and triple veins are formed on the transition to stable homogeneous veinless patterning. Therefore, the most pronounced vein structure falls within the range of $\sigma = 13$ to 27. Another way to visualize the formation of a vein, is to look at the evolution of auxin concentration with time for a column of cells perpendicular to the source-sink direction. As a vein forms, the auxin concentration in those cells will be less than the surrounding cells. A three-dimensional representation of the evolution of auxin concentration (s) with time for 1, 2 and 3 vein systems are given in Figures 3.6, 3.7 and 3.8, respectively.

When the switch is added to the line source system the same basic changes occur as for the point source system when the switch is added. The range for σ or the equivalent $\bar{\sigma}$ are slightly different when it comes to the number of veins formed. The boundary where a vein will form and where a vein does not form is of particular interest so the area around $\bar{\sigma}$=13 was investigated more closely. When a switch is added to the system where $\bar{\sigma}$=12.5 a vein is formed for some values of σ_h, σ_l, t_h and t_l. However, $\bar{\sigma}$=12 did not give a vein. The values of σ_h, σ_l, t_h and t_l at which a vein is formed for $\bar{\sigma}$=12.5 are given in Table 3.4 along with the time for vein formation to occur.

Veins also form more quickly when a switch is added to the system. When

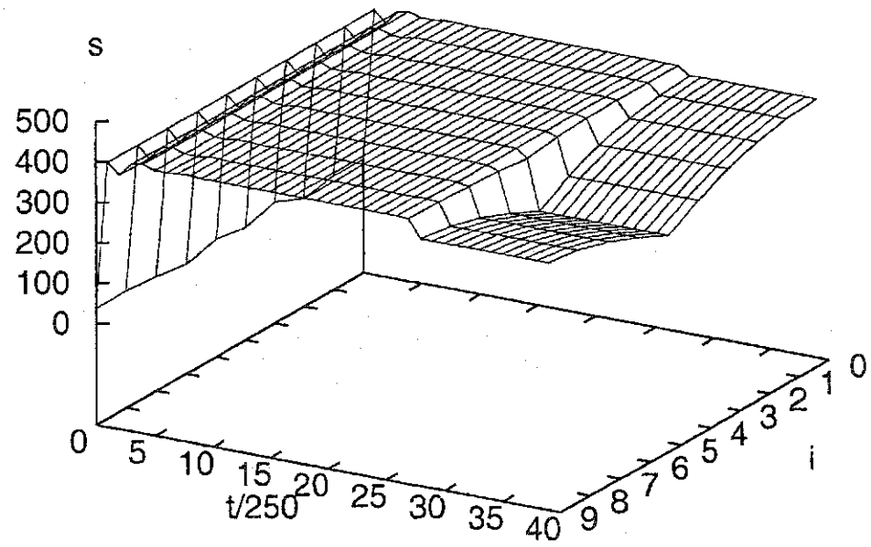

Figure 3.6: Evolution of auxin concentration (s) in time (t) for $\sigma = 13$, where i represents the cell (i,5) in the matrix. In this system one vein is formed. The vein is at the point of lowest auxin concentration.

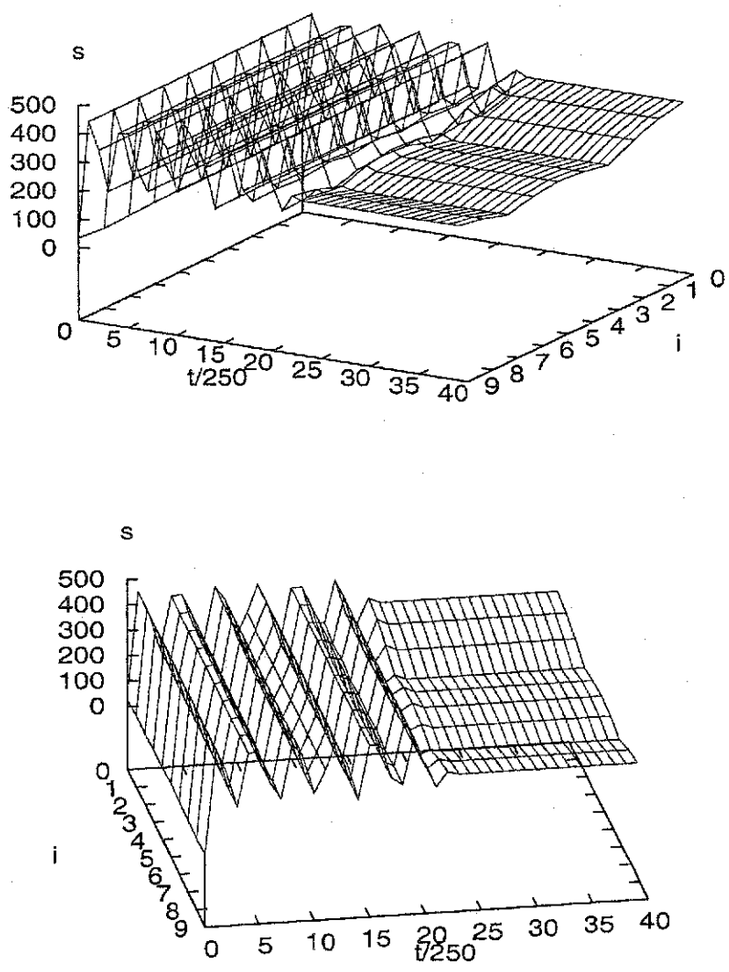

Figure 3.7: Evolution of auxin concentration (s) in time (t) for $\sigma = 15$, where i represents the cell (i,5) in the matrix. There are two views of the same data for visual clarity. In this system two veins are formed.

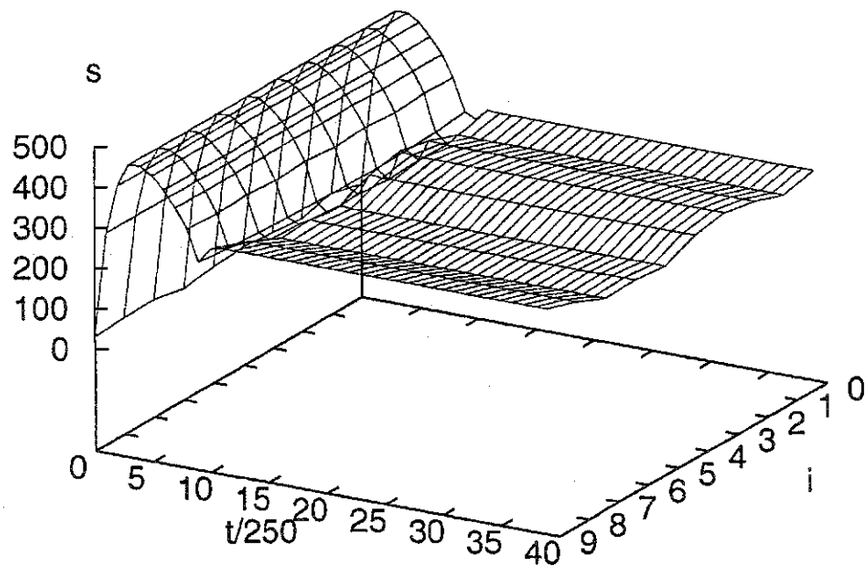

Figure 3.8: Evolution of auxin concentration (s) in time (t) for $\sigma = 19$, where i represents the cell (i,5) in the matrix. In this system three veins are formed.

Table 3.4: Vein formation time for $\bar{\sigma}$=12.5.

σ_h	σ_l	t_h	t_l	t
25	0	40	40	147252
25	0	50	50	56753
25	0	60	60	178060

looking at the systems with $\bar{\sigma}$=13-14.5 illustrated in Figure 3.9, it is clear to see that the switched systems form veins more quickly than the unswitched system. There also appear to be optimum parameter values that give the quickest time for a certain $\bar{\sigma}$. The only obvious difference between a system with $t_h = t_l = 20$ and for example $t_h = t_l = 50$ is the frequency of the fast oscillations in s, ϕ_2 or D_2 which is of course just equal to the frequency of the switching signal. As the value of $t_h = t_l$ increases past what is shown in Figure 3.9, vein formation no longer occurs. It appears that if the switching time is too long (especially for t_l), the system moves towards its homogeneous state which is the state it would go to with $\sigma_l = 0$. The system can then not move away from that homogeneous state after being switched back to the higher σ_h value.

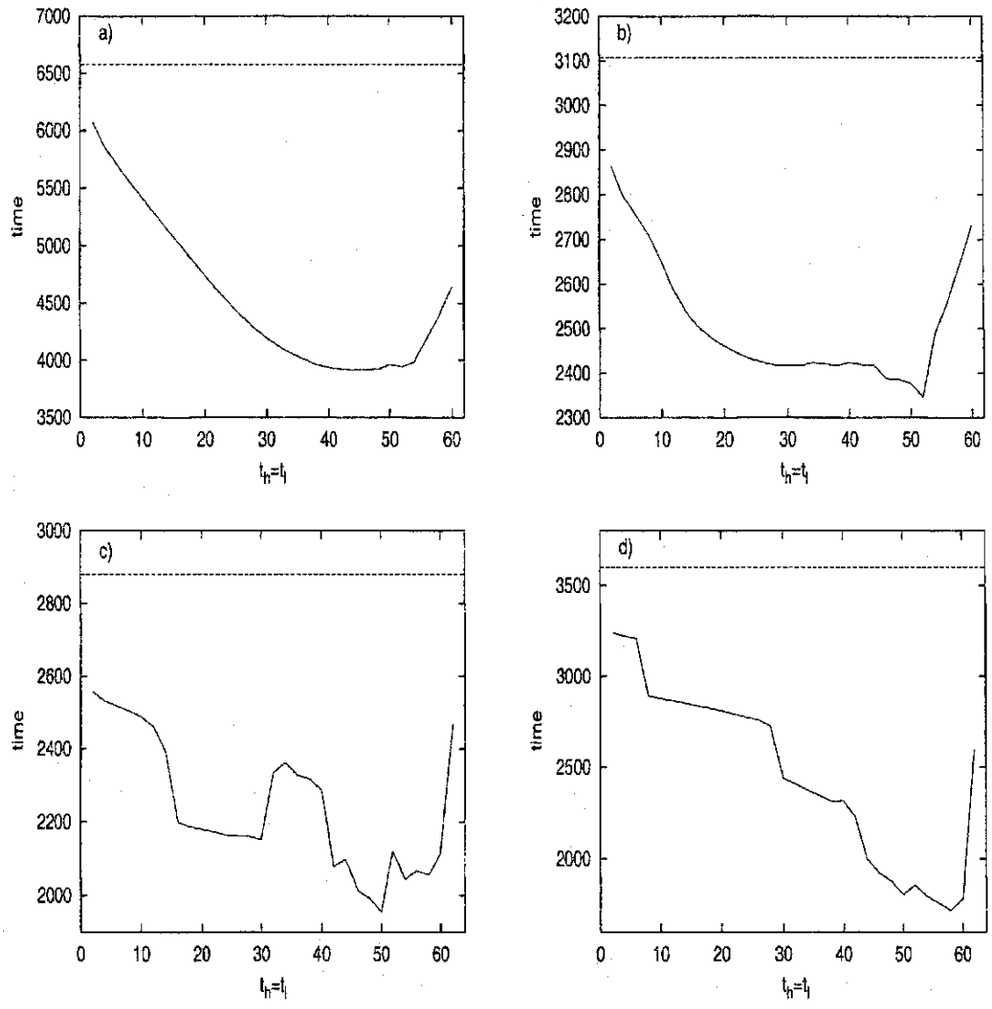

Figure 3.9: Examples of a vein forming faster with a switched system. The dotted line represents the time of vein formation for the unswitched system with a σ value equal to the switched systems $\bar{\sigma}$. a) The system with $\bar{\sigma} = 13$ with $\sigma_h = 26$ and $\sigma_l = 0$. b) The system with $\bar{\sigma} = 13.5$ with $\sigma_h = 27$ and $\sigma_l = 0$. c) The system with $\bar{\sigma} = 14$ with $\sigma_h = 28$ and $\sigma_l = 0$. d) The system with $\bar{\sigma} = 14.5$ with $\sigma_h = 29$ and $\sigma_l = 0$.

3.4.3 Model Exploration

The main goal that we had for this model was to undertake an initial exploration into how adding a switch would affect its dynamics. As such, many more questions arose from the results we obtained. Why did the systems show damped oscillations before the system destabilized and veins formed? Why did some switching parameters cause veins to form more quickly? Can we predict where a vein will form based on initial conditions?

Initially, the unswitched system was explored in more detail. The unswitched system displays oscillations in s, ϕ_2 and D_2 before a steady state is reached. (ϕ_1 and D_1 do not oscillate.) The values for s and ϕ_2 show the most dramatic changes. For s, the values tend to drop suddenly when a vein is formed, with the most significant decrease where the vein forms. For ϕ_2, the values where a vein forms increase dramatically and values between veins drop off significantly. An example of how s and ϕ_2 change in time are given in Figure 3.10. To study this dramatic change, the values of ϕ_2 for the vein and the two adjacent rows are looked at in more detail. Plots which are not shown here were done for the standard deviation of ϕ_2 matrix values versus time and the difference between the $\phi_2(m,n)$ for the vein and $\phi_2(m+1,n)$ and $\phi_2(m-1,n)$ versus time. Each method tried to make a distinction between the different rows before they appear to separate. The standard

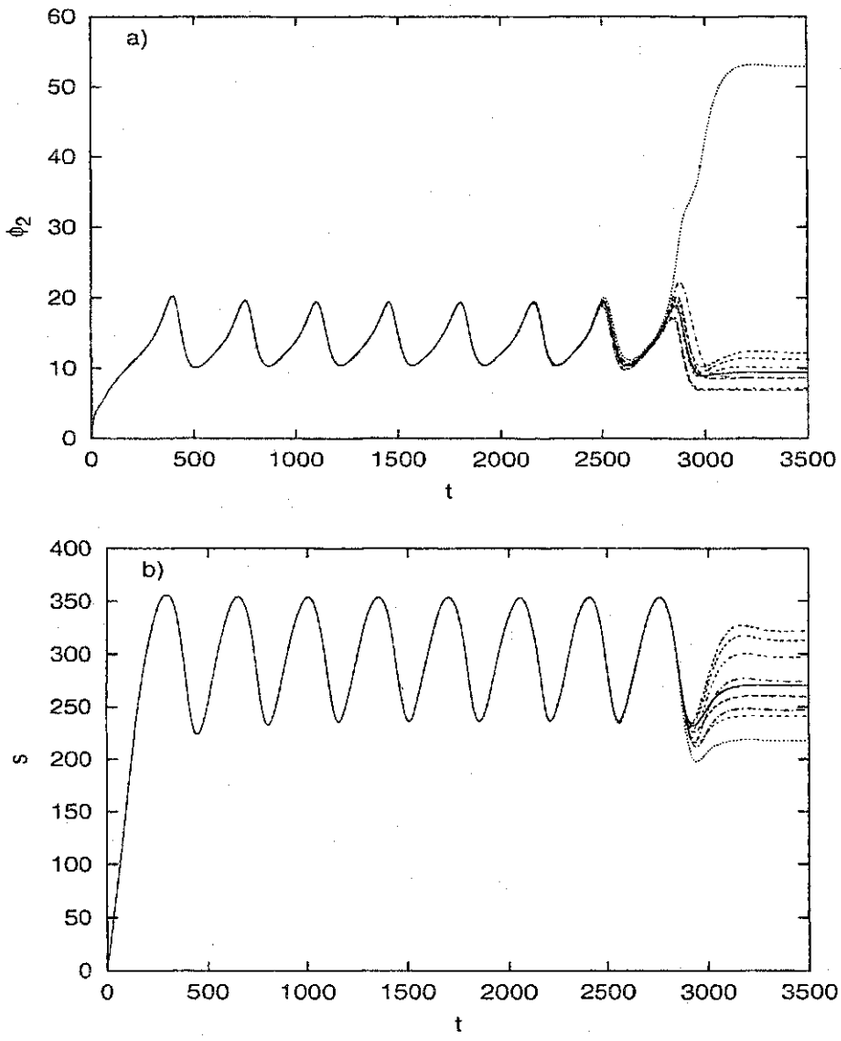

Figure 3.10: Evolution of $\phi_2(i,4)$ and $s(i,4)$ in time to compare where a vein is formed for a system with $\sigma = 14$. a) All ϕ_2 values in this column perpendicular to the source-sink direction follow a similar path until $t \approx 2500$ where a separation begins to occur. A vein is formed at $t \approx 2800$ where the flux in one particular cell increases dramatically compared to the rest. b) All s values in this column perpendicular to the source-sink direction follow a similar path until $t \approx 2800$ where all values decrease. The auxin concentration is the lowest where the vein forms.

deviation of all the values in the matrix was calculated to see how the values in the matrix changed in relation to one another. Were all the values of ϕ_2 similar, causing a jump in the standard deviation during vein formation? Was there any obvious increase in the standard deviation of the matrix sooner than what was obvious with the basic flux versus time plots for one flux? The standard deviation plots oscillated and increased dramatically at approximately the same time as the plot for one vein flux versus time. No real differences were observed. When looking at the difference between the flux in the vein and the rows adjacent to them, there appeared to be no significant difference between the two until just before the vein formed. Therefore, none of these methods helped give an early indication into which row would eventually differentiate into the vein. Since the initial values of auxin concentration in the matrix are allocated randomly, different ways of evaluating differences in auxin concentration were looked at to try and predict which row will eventually form a vein. The sum of auxin concentration for each row initially, and for a short initial time were calculated. However, the vein did not appear to form by any pattern I could discern. The vein did not always form in the row with highest or lowest sum of auxin concentration. There appeared to be no pattern in how the initial conditions affected where a vein would form.

Next, a similarity between the switched and unswitched systems was noticed. It appears that the intrinsic oscillation of the unswitched system is present in the switched system for a time as an average of its faster oscillations. However, the switched system forms a vein more quickly. The final steady state of the unswitched system is also the same as the average steady state of the smaller oscillations of the switched system. This is illustrated in Figure 3.11. The average of the smaller switched oscillations follows the intrinsic oscillations of the unswitched system. From this result more questions arose. Was the oscillation in the unswitched system a result of the two-dimensional spatial interactions, or could oscillations occur in a one-dimensional array? And was the switching frequency yielding the minimum time for vein formation related to the frequency of these intrinsic oscillations?

To investigate the first question, one-dimensional arrays of cells were studied. When the system is reduced to a 1xn matrix for $n = 2..5$, the system is simple enough that eigenvalues[8] can be calculated easily. The eigenvalues were calculated using the Xppaut software.[104] The eigenvalues for these systems are given in Table 3.5. The steady states about which they are calculated are given in Table 3.6. For all the systems discussed in this table, each have eigenvalues with only negative real parts. This means that each system is an attractor, which means

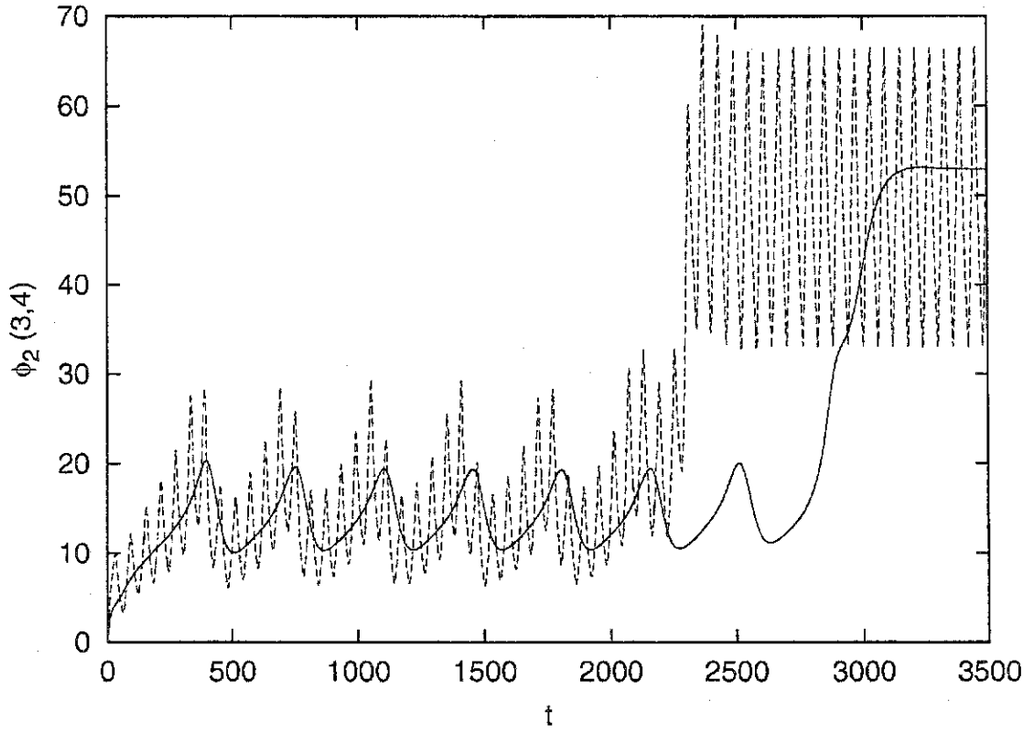

Figure 3.11: Comparing $\phi_2(3,4)$ for both switched and unswitched systems. The sudden increase in flux for both systems signals vein formation. The solid line is the unswitched system with $\sigma = 14$ and the dashed line is the switched system with $\sigma_h = 28$, $\sigma_l = 0$, $t_h = 30$, $t_l = 30$ and $\bar{\sigma} = 14$.

Table 3.5: Eigenvalues for the reduced system of 1xn matrices.

1x2 matrix	1x3 matrix
-0.092846	$-0.035729+0.062199i$
-0.144861	$-0.035729-0.062199i$
	-0.057147
	-0.615803
1x4 matrix	**1x5 matrix**
$-0.010995+0.050530i$	$-0.000578+0.040413i$
$-0.010995-0.050530i$	$-0.000578-0.040413i$
-0.055479	-0.054955
-0.064912	-0.058228
-0.322076	-0.092844
-0.786655	-0.144863
	-0.541896
	-0.863872

Table 3.6: Steady states for the reduced systems of 1xn matrices. The variable s_c refers to the auxin concentration of the source cell. The variables s_i, where i=1..3, are labeled with s_1 being the auxin concentration of the cell next to the sink, with neighbouring cell up to the source given the next integer. The variables D_i, where i=1..4, are labeled with D_1 being the diffusion coefficient between the sink and the neighbour cell and i increases for the diffusion coefficients between the next neighbouring cells up to the source.

1x2 matrix	1x3 matrix
$s_c = 70.633$	$s_c = 141.27$
$D_1 = 0.26899$	$s_1 = 70.633$
	$D_{1-2} = 0.26899$
1x4 matrix	**1x5 matrix**
$s_c = 211.9$	$s_c = 282.53$
$s_2 = 141.27$	$s_3 = 211.9$
$s_1 = 70.633$	$s_2 = 141.27$
$D_{1-3} = 0.26899$	$s_1 = 70.633$
	$D_{1-4} = 0.26899$

they all go towards a steady state. The 1x2 matrix system has no imaginary parts in its eigenvalues which shows that no oscillation occurs in this example as it goes towards its steady state. However, the other longer arrays have imaginary parts that correspond to damped oscillations. Thus, oscillations are not dependent on the two-dimensional aspect. It appears that oscillations occur because as auxin concentrations increase, so too does the diffusion coefficient and flux, causing auxin to flow quickly out of the cell. As the auxin concentration decreases, so too do the diffusion coefficient and flux, causing auxin to leave the cell more slowly. This causes auxin concentration to again accumulate, and this cycles until a steady state is reached. Figure 3.12 shows the evolution of flux in time near the sink for the 1xn matrices. There are some other features of these systems that can be predicted by the eigenvalues. The real parts of the complex eigenvalues get less negative as the length of the array increases. This means that the oscillations will take longer to damp out. The 1x5 matrix has the least negative real part for its complex eigenvalues, and it does take longer for its oscillations to damp out. Also, the imaginary parts of the complex eigenvalues get smaller as the length of the array increases. This predicts that the system with the smaller imaginary part will have a larger frequency. The 1x5 matrix has the smallest imaginary part for its complex eigenvalues, and it does have a larger frequency than the shorter

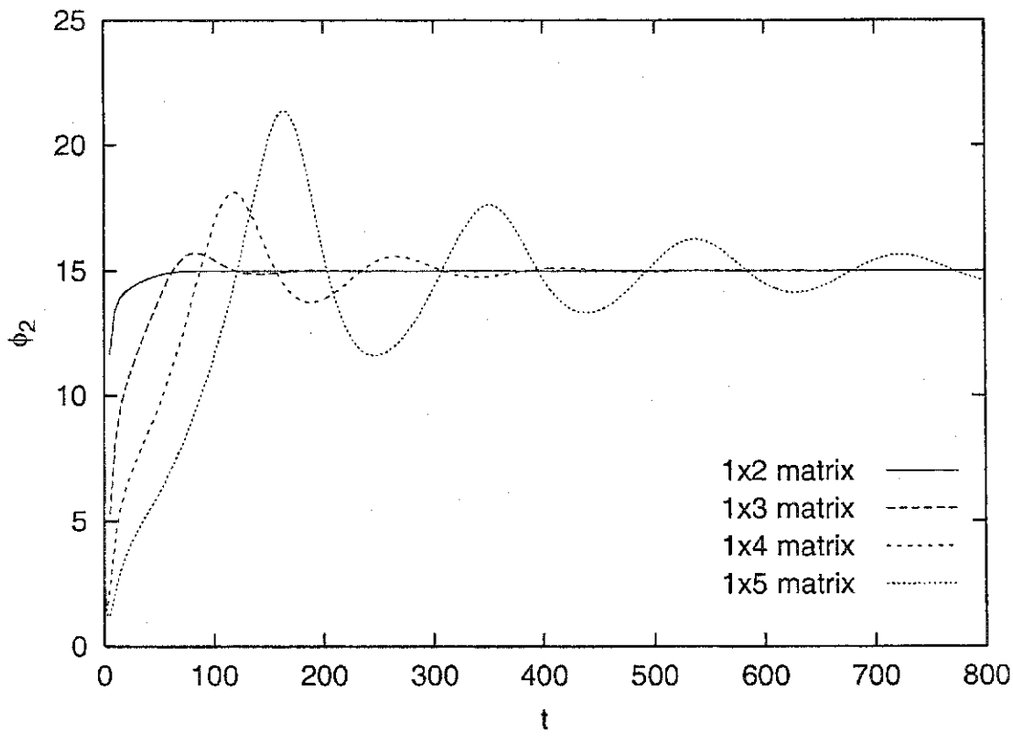

Figure 3.12: Comparing ϕ_2 near the sink for the reduced systems of 1xn matrices with $\sigma = 15$.

arrays.

To answer the second question of whether the switching frequency yielding the minimum time for vein formation is related to the frequency of the unswitched oscillations, the frequency of unswitched oscillations were calculated and compared with the switching frequencies. This was done to see if tuning the pulse of auxin production to some multiple of the natural oscillation frequency would give the optimum switching time to produce a vein the quickest. Since we mostly compared switches that have equal t_h and t_l and a $\sigma_l = 0$, the value of σ_h is always double the σ value that is compared for switched and unswitched systems. Therefore, the frequencies of the unswitched systems calculated were for σ equal to $\bar{\sigma}$ and σ_h. For example, if we compared the systems of $\sigma = \bar{\sigma} = 13$, the value of σ_h was 26. We calculated the natural oscillation frequency at $\sigma = 13$ because the final vein patterns tended to be similar for unswitched and switched systems with equal σ and $\bar{\sigma}$. We also calculated the natural oscillation frequency at $\sigma = 26$ because the switched system has $\sigma = 26$ when the switch is at its high value and the switching frequency might be related to the natural oscillation frequency of the high switched value. There are no oscillations when $\sigma = 0$, so we did not need to compare the low switch value of σ. Values were calculated and compared for σ equal to 13, 15 and 19. The results are not shown, but there was no simple

common multiple for the natural oscillation frequency of the unswitched systems and the switching frequency that yielded the minimum time for vein formation.

The exploration of this model has given many interesting results as well as more questions that need to be answered in future work. In the unswitched system, there are damped oscillations. An instability occurs and this instability causes vein formation to occur. The system then reaches a stable steady state. This is similar behaviour to that seen in Turing instabilities.[105,106] Turing describes a system that is originally quite homogeneous, that then may eventually develop a stable pattern or structure because of an instability in the homogeneous equilibrium. This instability may be triggered by random disturbances. Our model starts off with initial random conditions, becomes quite homogeneous, then an instability occurs and a stable vein formation pattern emerges quite suddenly. The damped oscillations are independent of the two-dimensional spatial structure of the matrix, and occur with a linear array of at least a 1x3 matrix. The switched systems forms veins more quickly than the comparable unswitched systems. There are also optimum parameter values which give the quickest vein formation. The average of the smaller switched oscillations follow the intrinsic oscillations of the unswitched system. A vein is then formed in the switched system sooner than the unswitched system. There appears to be no correlation between the natural oscil-

lation frequency and the switch frequency for the optimum parameter values. This leaves us with many questions that could be the setting for future work. How does periodic switching affect the speed of vein formation? What factor contributes to the optimum parameter values which give the minimum time for vein formation? Does the periodic switch need to be functioning the whole time, or does initial switching followed by a constant σ also speed up vein formation?

Chapter 4

Conclusion

Rhythms and time keeping mechanisms are essential to life.[13,16] Some rhythms are periodic and some are aperiodic. Both have important roles and implications in life. The focus here has been on periodic rhythms, and their involvement in two different systems. The first dealt with a very simple model of cell division. This original model by Novak and Tyson[45] did not take into account any ultradian rhythms that have been associated with cell division.[19,22,23] To try and model a type of ultradian rhythm, we added a periodic switch, that switched the system between a stable fixed point and a stable limit cycle. Adding the switch gave some new interesting dynamics that were not seen in the model before the switch. Entrainment, quasi-periodicity and chaos were all different types of behaviours that could be modeled with different switching parameters. Future work on this model could include a closer investigation into the fractal nature of the chaotic

islands in the parameter plane. We could change the shape of the periodic forcing function to compare any differences or similarities in the behaviour of the model. Does the shape of the periodic forcing function influence the type of entrainment, or the size of the chaotic regions?

The second system dealt with a very simple vein formation model. The original model by Mitchison[101] had the hormone auxin produced and released at a constant rate. Many hormones are released in a pulsatile manner,[25,30] and so we added our switch to this auxin production term to model that type of hormone release. Adding the switch gave the interesting result of veins forming in the matrix sooner than the equivalent unswitched system. Our understanding of why veins form more quickly when auxin production in the source is pulsed is unclear. Future work on this model could be to find out why veins form at all, and why a periodic forcing term would form veins more quickly. Changing the shape of the forcing function to see if veins still form more quickly, would also be interesting. Much more work still needs to be done with this driven model. Our goal here was to open the door.

Appendix A

Implicit Runge-Kutta Method

A.1 Derivation

The Runge-Kutta method is a higher order numerical method for solving differential equations that is derived by manipulating the Taylor series.[107] This form of the Runge-Kutta method has the property that the right-hand sides can be calculated explicitly. For some systems of equations, using an explicit method does not give correct results unless a very small stepsize is used. To overcome this problem implicit methods were developed. The implicit method chosen to study the cell division cycle model was the second order implicit Runge-Kutta method[71] which is defined by:

$$t_{n+1} = t_n + h, \tag{A.1}$$

$$y_{n+1} = y_n + \frac{1}{4}(k_1 + 3k_2), \tag{A.2}$$

where

$$k_1 = hf(t_n, y_n - k_1 + k_2), \tag{A.3}$$

$$k_2 = hf(t_n + \frac{2}{3}h, y_n + \frac{2}{3}k_2) \tag{A.4}$$

where h is the stepsize.

A.2 Implementation

The algorithm used to take one step of the implicit Runge-Kutta method of size h, consists of several parts. First, the vector k_2 needs to be calculated. Since k_2 appears on both the right and left hand sides of equation A.4, two new vectors need to be defined. Therefore we define $k_2^{\text{new}} = hf(t_n + \frac{2}{3}h, y_n + \frac{2}{3}k_2^{\text{old}})$, choose an initial guess for the value of k_2^{old} and iterate until the vector $k_2^{\text{new}} \simeq k_2^{\text{old}}$. The vector k_2 is then given the value of k_2^{new}. Next, the vector k_1 needs to be calculated in a similar fashion. Therefore we define $k_1^{\text{new}} = hf(t_n, y_n - k_1^{\text{old}} + k_2)$, choose an initial guess for the value of k_1^{old} and iterate until the vector $k_1^{\text{new}} \simeq k_1^{\text{old}}$. The vector k_1 is given the value of k_1^{new}. Once k_1 and k_2 are calculated, the vector y_{n+1} is calculated by equation A.2. Finally, t_n is incremented by the stepsize h, and another step can be calculated in the same manner.

Bibliography

[1] Dieter Armbruster and Marguerite George. Parametrically forced pattern formation. *Chaos*, 11(1):52–56, 2001.

[2] Mario Feingold, Diego L. Gonzalez, Oreste Piro, and Hector Viturro. Phase locking, period doubling, and chaotic phenomena in externally driven excitable systems. *Phys. Rev. A*, 37(10):4060–4063, 1988.

[3] Leon Glass and Jiong Sun. Periodic forcing of a limit-cycle oscillator: Fixed points, arnold tongues, and the global organization of bifurcations. *Phys. Rev. E*, 50(6):5077–5084, 1994.

[4] John Guckenheimer and Philip Holmes. *Nonlinear Oscillations, Dynamical Systems, and Bifurcations of Vector Fields*. Springer-Verlag New York Inc., 1983.

[5] Bai-Lin Hao. Two kinds of entrainment-beating transitions in a driven limit-cycle oscillator. *J. Theor. Biol.*, 98:9–14, 1982.

[6] P. Parmananda and Yu Jiang. Synchronization of chemical systems using external forcing. *J. Phys. Chem. A*, 102:4532–4536, 1998.

[7] Arkady S. Pikovsky, Michael G. Rosenblum, Grigory V. Osipov, and Jürgen Kurths. Phase synchronization of chaotic oscillators by external driving. *Physica D.*, 104:219–238, 1997.

[8] Steven H. Strogatz. *Nonlinear Dynamics and Chaos: With Applications to Physics, Biology, Chemistry, and Engineering*. Addison-Wesley Publishing Com., 1994.

[9] James A. Blackburn. Experiments in nonlinear electronic and mechanical systems. *Physics in Canada*, 57:99–105, 2001.

[10] Y. Braiman and I. Goldhirsch. Taming chaotic dynamics with weak periodic perturbations. *Phys. Rev. Lett.*, 66:2545–2548, 1991.

[11] Albert Goldbeter. *Biochemical oscillations and cellular rhythms*. Cambridge University Press, 1996.

[12] F. C. Hoppensteadt and J. Keener. Phase locking of biological clocks. *J. Math. Biol.*, 15:339–349, 1982.

[13] Beatrice M. Sweeney. *Rhythmic Phenomena in Plants*. Academic Press, Inc., 1987.

[14] Jon W. Jacklet and Jeffrey Geronimo. Circadian rhythm: Population of interacting neurons. *Science*, 174:299–302, 1971.

[15] David Lloyd. Circadian and ultradian clock-controlled rhythms in unicellular microorganisms. *Adv. Microb. Physiol.*, 39:291–337, 1998.

[16] Leon Glass and Michael C. Mackey. *From Clocks to Chaos: The Rhythms of Life*. Princeton University Press, 1988.

[17] Didier Gonze and Albert Goldbeter. Entrainment versus chaos in a model for a circadian oscillator driven by light-dark cycles. *J. Stat. Phys.*, 101:649–663, 2000.

[18] F. Kippert and P. Hunt. Ultradian clocks in eukaryotic microbes: from behavioural observation to functional genomics. *Bioessays*, 22:16–22, 2000.

[19] David Lloyd and E.I. Volkov. Quantized cell cycle times: interaction between a relaxation oscillator and an ultradian clock pulses. *Biosystems*, 23:305–310, 1990.

[20] David Lloyd. Chaos and ultradian rhythms. *Biol. Rhythm Res.*, 28:134–143, 1997.

[21] David Lloyd and Ernest L. Rossi, editors. *Ultradian rhythms in Life Processes: An inquiry into fundamental principles of chronobiology and psychobiology*. Springer-Verlag, 1992.

[22] Leland N. Edmonds, Jr. and Kenneth J. Adams. Clocked cell cycle clocks. *Science*, 211:1002–1013, 1981.

[23] Steven B. Haase and Steven I. Reed. Evidence that a free-running oscillator drives g1 events in the budding yeast cell cycle. *Nature*, 401:394–397, 1999.

[24] C. Robertson McClung. Circadian rhythms in plants. *Annu. Rev. Plant. Physiol. Plant Mol. Biol.*, 52:139–162, 2001.

[25] S.H. Song, L. Kjems, R. Ritzel, S.M. McIntyre, M.L. Johnson, J.D. Veldhuis, and P.C. Butler. Pulsatile insulin secretion by human pancreatic islets. *J. Clin. Endocrinol. Metab.*, 87:213–221, 2002.

[26] James E. Ferrell, Jr. How regulated protein translocation can produce switch-like responses. *Trends Biochem. Sci.*, 23:461–465, 1998.

[27] James E. Ferrell, Jr. and Eric M. Machleder. The biochemical basis of an all-or-none cell fate switch in *Xenopus* oocytes. *Science*, 280:895–898, 1998.

[28] Joshua L. Cherry and Frederick R. Adler. How to make a biological switch. *J. Theor. Biol.*, 203:117–133, 2000.

[29] Timothy S. Gardner, Charles R. Cantor, and James J. Collins. Constuction of a genetic toggle switch in *Escherichia coli*. *Nature*, 403:339–342, 2000.

[30] J.D. Veldhuis. A parsimonious model of amplitude and frequency modulation of episodic hormone secretory bursts as a mechanism for ultradian signalling by endocrine glands. In Lloyd and Rossi,[21] pages 139–172.

[31] Subir K. Sarkar. Information dimension for quasiperiodic trajectories with quadratically irrational winding number. *Phys. Lett.*, 106A(3):95–98, 1984.

[32] A. Murray and T. Hunt. *The Cell Cycle, an Introduction*. Oxford University Press, 1993.

[33] Duncan J. Clarke and Juan F. Giménez-Abián. Checkpoints controlling mitotis. *BioEssays*, 22:351–363, 2000.

[34] C. Hutchison and D.M. Glover. *Cell Cycle Control.* Oxford University Press, 1995.

[35] Kurt W. Kohn. Molecular interaction map of the mammalian cell cycle control and dna repair systems. *Mol. Biol. Cell*, 10:2703–2734, 1999.

[36] G. Bard Ermentrout. The mathematics of biological oscillators. *Methods Enzymol.*, 240:198–216, 1994.

[37] Katherine C. Chen, Attila Csikasz-Nagy, Bela Gyorffy, John Val, Bela Novak, and John J. Tyson. Kinetic analysis of a molecular model of the budding yeast cell cycle. *Mol. Biol. Cell*, 11:369–391, 2000.

[38] Albert Goldbeter. A minimal cascade model for the mitotic oscillator involving cyclin and cdc2 kinase. *Proc. Natl. Acad. Sci.*, 88:9107–9111, 1991.

[39] A. Goldbeter and J.M. Guilmot. Arresting the mitotic oscillator and the control of cell proliferation: Insights from a cascade model for cdc2 kinase activation. *Experientia*, 52(3):212–216, 1996.

[40] David Lloyd, Alun L. Lloyd, and Lars Folke Olsen. The cell division cycle: a physiologically plausible dynamic model can exhibit chaotic solutions. *Biosystems*, 27:17–24, 1992.

[41] Bela Novak and John J. Tyson. Quantitative analysis of a molecular model of mitotic control in fission yeast. *J. Theor. Biol.*, 173:283–305, 1995.

[42] John J. Tyson, Bela Novak, Garrett M. Odell, Kathy Chen, and C. Dennis Thron. Chemical kinetic theory: understanding cell cycle regulation. *Trends Biochem. Sci.*, 21:89–96, 1996.

[43] Zuohuan Zheng, Tianshou Zhou, and Suochun Zhang. Dynamical behavior in the modeling of the cell division cycle. *Chaos, Solitons and Fractals*, 11:2371–2378, 2000.

[44] Peter H. Raven and George B. Johnson. *Biology: 6th Edition.* McGraw-Hill Com., 2002.

[45] Bela Novak and John J. Tyson. Modelling the cell division cycle: M-phase trigger, oscillations, and size control. *J. Theor. Biol.*, 165:101–134, 1993.

[46] C.D. Thron. A model for a bistable biochemical trigger of mitosis. *Biophys. Chem.*, 57:239–251, 1996.

[47] J. M. Mitchison. The growth of single cells i. *Schizosaccharomyces pombe. Exp. cell res.*, 13:244–262, 1957.

[48] P. Nurse, P. Thuriaux, and K. Nasmyth. Genetic control of the cell division cycle in fission yeast *Schizosaccharomyces pombe. Mol. Gen. Genet.*, 146:167–178, 1976.

[49] M. J. Lohka, M. K. Hayes, and J. L. Maller. Purification of maturation-promoting factor, an intracellular regulator of early mitotic events. *Proc. Natl. Acad. Sci. USA*, 85:3009–3013, 1988.

[50] Andrew W. Murray and Marc W. Kirschner. Dominoes and clocks: The union of two views of the cell cycle. *Science*, 246:614–621, 1989.

[51] Andrew W. Murray, Mark J. Solomon, and Marc W. Kirschner. The role of cyclin synthesis and degradation in the control of maturation promoting factor activity. *Nature*, 339:280–286, 1989.

[52] John J. Tyson, Bela Novak, Kathy Chen, and John Val. Checkpoints in the cell cycle from a modeler's perspective. *Prog. Cell Cycle Res.*, 1:1–8, 1995.

[53] Timothy S. Gardner, Milos Dolnik, and James J. Collins. A theory for controlling cell cycle dynamics using a reversibly binding inhibitor. *Proc. Natl. Acad. Sci.*, 95:14190–14195, 1998.

[54] Michael Polymenis and Emmett V. Schmidt. Coordination of cell growth with cell division. *Curr. Opin. Genet. Dev.*, 9:76–80, 1999.

[55] James E. Ferrell, Jr. Tripping the switch fantastic: how a protein kinase cascade can convert graded inputs into switch-like outputs. *Trends Biochem. Sci.*, 21:460–466, 1996.

[56] Martin F. Testorf, Annika M. Karlsson, Samuel P. S. Svensson, P. Åke Öberg, and Ingemar Lundström. A model for switch-like phenomena in biological systems. *Biophys. Chem.*, 94:1–9, 2001.

[57] Donald Price, Simon Rabinovitch, Patrick H. O'Farrell, and Shelagh D. Campbell. *Drosophila wee1* has an essential role in the nuclear divisions of early embryogenesis. *Genetics*, 155:159–166, 2000.

[58] P. Russell and P. Nurse. Negative regulation of mitosis by $wee1^+$, a gene encoding a protein kinase homolog. *Cell*, 49:559–567, 1987.

[59] L. N. Edmunds, Jr. *Cell Cycle Clocks*. Marcel Dekker, Inc., 1984.

[60] F. Kippert and D. Lloyd. A temperature-compensated ultradian clock ticks in *Schizosaccharomyces pombe*. *Microbiology*, 141:883–890, 1995.

[61] A. L. Lloyd and D. Lloyd. Chaos: Its significance and detection in biology. *Biol. Rhythm Res.*, 26:233–252, 1995.

[62] Taunia L.L. Closson and Marc R. Roussel. Synchronization by irregular inactivation. *Phys. Rev. Lett.*, 85(18):3974–3977, 2000.

[63] Taunia L.L. Closson, Brian R. Greenhalgh, Janice L. McMurchy, and Marc R. Roussel. Parametrically driven cell division cycle oscillators: Entrainment and chaos. *In Progress*.

[64] Govindan Rangarajan, Salman Habib, and Robert D. Ryne. Lyapunov exponents without rescaling and reorganization. *Phys. Rev. Lett.*, 80(17):3747–3750, 1998.

[65] Leon Glass and C. P. Malta. Chaos in multi-looped negative feedback systems. *J. Theor. Biol.*, 145:217–223, 1990.

[66] Carsten Knudsen. Topological winding numbers for period-doubling cascades. *Int. J. Bifurcation and Chaos*, 6(1):185–187, 1996.

[67] Wei Wang and Xi-Xian Yao. Generalized winding number of a dynamical system. *Commun. Theor. Phys.*, 17(1):89–92, 1992.

[68] N. Metropolis, M. L. Stein, and P. R. Stein. On finite limit sets for transformations on the unit interval. *J. Combin. Theor.*, 15:25–44, 1973.

[69] J. Tyson and S. Kauffman. Control of mitosis by a continuous biochemical oscillation: Synchronization; spatially inhomogeneous oscillations. *J. Math. Biol.*, 1:289–310, 1975.

[70] Kiyosi Itô, editor. *Encyclopedic Dictionary of Mathematics*, volume 2. The MIT Press, second edition, 1993.

[71] G. William Gear. *Numerical Initial Value Problems in Ordinary Differential Equations*. Prentice-Hall, Inc., 1971.

[72] M. R. Guevara, L. Glass, and A. Shrier. Phase locking, period doubling bifurcations and irregular dynamics in periodically stimulated cardiac cells. *Science*, 214:1350–1353, 1981.

[73] C. Graves, L. Glass, D. Laporta, R. Meloche, and A. Grassino. Respiratory phase locking during mechanical ventilation in anesthetized human subjects. *Am. J. Physiol.*, 250:R902–909, 1986.

[74] G. A. Petrillo, L. Glass, and T. Trippenbach. Phase locking of the respiratory rhythm in cats to a mechanical ventilator. *Can. J. Physiol. Pharmacol.*, 61:599–607, 1983.

[75] Manuel Rotenberg. Selective synchrony of cells of differing cycle times. *J. Theor. Biol.*, 66:389–398, 1977.

[76] Steven H. Strogatz and Ian Stewart. Coupled oscillators and biological synchronization. *Sci. Am.*, 269:102–107, 1993.

[77] V. P. Zhdanov and B. Kasemo. Synchronization of metabolic oscillations: Two cells and ensembles of absorbed cells. *J. Biol. Phys.*, 27:295–311, 2001.

[78] Robert E. Ecke, J. Doyne Farmer, and David K. Umberger. Scaling of the arnold tongues. *Nonlinearity*, 2:175–196, 1989.

[79] A. L. Goldberger, V. Bhargava, B. J. West, and A. J. Mandell. On a mechanism of cardiac electrical stability: The fractal hypothesis. *Biophys. J.*, 48:525–528, 1985.

[80] Dante R. Chialvo, André Longtin, and Johannes Müller-Gerking. Stochastic resonance in models of neuronal ensembles. *Phys. Rev. E*, 55(2):1798–1808, 1997.

[81] Charles M. Gray and David A. McCormick. Chattering cells: Superficial pyramidal neurons contributing to the generation of synchronous oscillations in the visual cortex. *Science*, 274:109–113, 1996.

[82] Steve Fiering, Emma Whitelaw, and David I. K. Martin. To be or not to be active: the stochastic nature of enhancer action. *Bioessays*, 22:381–387, 2000.

[83] Akos Sveiczer, John J. Tyson, and Bela Novak. A stochastic, molecular model of the fission yeast cell cycle: role of the nucleocytoplasmic ratio in cycle time regulation. *Biophys. Chem.*, 92:1–15, 2001.

[84] M. R. Guevara and L. Glass. Phase locking, period doubling bifurcations and chaos in a mathematical model of a periodically driven oscillator: A theory for entrainment of biological oscillators and the generation of cardiac dysrhythmias. *J. Math. Biol.*, 14:1–23, 1982.

[85] Peter H. Raven, Ray. F. Evert, and Susan E. Eichhorn. *Biology of Plants*. Worth Publishers, Inc., fourth edition, 1986.

[86] Peter J. Davies, editor. *Plant Hormones: Physiology, Biochemistry and Molecular Biology.* Kluwer Academic Publishers, Netherlands, 1995.

[87] Robert S. Bandurski, Jerry D. Cohen, Janet P. Slovin, and Dennis M. Reinecke. Auxin biosynthesis and metabolism. In Davies,[86] pages 39–65.

[88] Robert E. Cleland. Auxin and cell elongation. In Davies,[86] pages 214–227.

[89] Roni Aloni. The induction of vascular tissue by auxin and cytokinin. In Davies,[86] pages 531–546.

[90] Abraham D. Krikorian. Hormones in tissue culture and micropropagation. In Davies,[86] pages 774–796.

[91] Terri L. Lomax, Gloria K. Muday, and Philip H. Rubery. Auxin transport. In Davies,[86] pages 509–530.

[92] Peter B. Kaufman, Liu-Lai Wu, Thomas G. Brock, and Donghern Kim. Hormones and the orientation of growth. In Davies,[86] pages 547–571.

[93] Thomas Gianfagna. Natural and synthetic growth regulators and their use in horticultural and agronomic crops. In Davies,[86] pages 751–773.

[94] James D. Metzger. Hormones and reproductive development. In Davies,[86] pages 617–648.

[95] Charles Darwin and Francis Darwin. *The power of movement in plants*. Da Capo Press, New York, 1966.

[96] F. W. Went. On growth-accelerating substances in the coleoptile of *Avena sativa*. *Proc. Sec. Sci. Kon. Aka. van Wetenschappen te Amsterdam*, 30:10–19, 1926.

[97] A. J. Haagen-Smit, W. B. Dandliker, S. H. Wittwer, and A. E. Murneek. Isolation of 3-indoleacetic acid from immature corn kernels. *Am. J. Bot.*, 33:118–120, 1946.

[98] T. Sachs. Polarity and the induction of organized vascular tissues. *Ann. Bot.*, 33:263–275, 1968.

[99] T. Sachs. Patterned differentiation in plants. *Differentiation*, 11:65–73, 1978.

[100] T. Sachs. The induction of transport channels by auxin. *Planta*, 127:201–206, 1975.

[101] G. J. Mitchison. A model for vein formation in higher plants. *Proc. R. Soc. Lond. B.*, 207:79–109, 1980.

[102] A. V. Hill. The possible effects of the aggregation of the molecules of haemoglobin on its dissociation curves. *J. Physiol. (Lond.)*, 40:iv–vii, 1910.

[103] George Marsaglia and Arif Zaman. Some portable very-long-period random number generators. *Comput. Phys.*, 8:117–121, 1994.

[104] Bard Ermentrout. Xppaut4.0, May 2000.

[105] Razvan A. Satnoianu, Michael Menzinger, and Philip K. Maini. Turing instabilities in general systems. *J. Math. Biol.*, 41:477–492, 2000.

[106] A. M. Turing. The chemical basis of morphogenesis. *Phil. Trans. R. Soc. Lond. B*, 237:37–72, 1952.

[107] R. Kent Nagle and Edward B. Saff. *Fundamentals of Differential Equations: Third Edition.* Addison-Wesley Publishing Com., 1993.